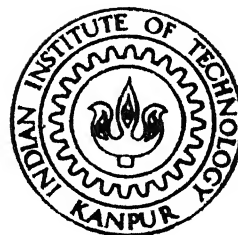# Numerical Simulation of Turbulent Flow Past a Backward Facing Step and Through a Parallel Plate Channel

by

LOKHANDE BIPIN SURESH

DEPARTMENT OF MECHANICAL ENGINEERING

INDIAN INSTITUTE OF TECHNOLOGY KANPUR

MARCH, 1997

Numerical Simulation of Turbulent Flow Past a Backward Facing Step and Through a Parallel Plate Channel

Thesis Submitted
in Partial Fulfillment of the Requirements
for the Degree of
Master of Technology

by

Lokhande Bipin Suresh

to the

DEPARTMENT OF MECHANICAL ENGINEERING
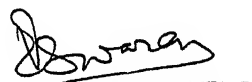INDIAN INSTITUTE OF TECHNOLOGY KANPUR
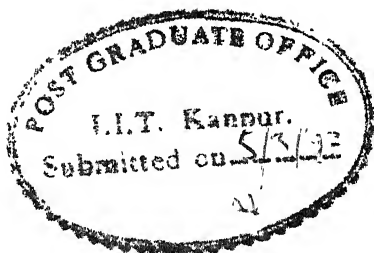March, 1997

ME-1997-M-LCK-NUM

CERTIFICATE

CERTIFIED that the thesis entitled, " NUMERICAL SIMULATION OF TURBULENT FLOW PAST A BACKWARD FACING STEP AND THROUGH A PARALLEL PLATE CHANNEL" has been submitted by Lokhande Bipin Suresh under our supervision and that this work has not been submitted elsewhere for award of a degree.

Dr. V. Eswaran
Associate Professor
Department of Mechanical Engineering
INDIAN INSTITUTE OF TECHNOLOGY
KANPUR-208016

Dr. G. Biswas
Professor
Department of Mechanical Engineering
INDIAN INSTITUTE OF TECHNOLOGY
KANPUR-208016

March, 1997

Acknowledgement

Abstract

The present work deals with the the *numerical simulation of turbulent flow using a finite volume method and a standard $k - \epsilon$ model.* A standard $k - \epsilon$ model was incorporated in the laminar code and was applied on two test cases 1) Channel flow 2) Backward facing step flow. The code is three dimensional and can simulate a flow in a any irregular geometries. The equations are solved in a physical domain thus avoiding a need for transformation of governing equations.

The accuracy of determining the turbulent flow field depends upon the type of numerical scheme used. The code is dveloped for 3-D applications but the present computaions were done using the 2-D modification. The present work has demonstrated the ability of the method used to predict the turbulent flow field correctly. Standard $k - \epsilon$ model is seen to establish good compromise between accuracy and computational cost. The results of flow over a backward-facing step are seen to be in good aggrement with the experimental as well as other advance turbulence model results. In fact it was observed that the present results was able to capture the secondary recirculation zone which previous computation with the same model failed. The length of primary recirculation zone obtained is $6.0H$ which is found to be in good aggrement with the experimental results of Kim *et al*[37] for which the length is $7.0H$. Also the secondary recirculation length obtained is $0.83H$ which also aggres well with the length obtained by Lien and Leschziner[40] which is $1.0H$ using a Reynolds stress model.

Contents

List of Figures

Nomenclature

Latin Symbols

$C_\mu, C_{\epsilon 1}, C_{\epsilon 2}$	constants in turbulence model of equation(3.15,316 and 317)
E	constant having a value of 9.0 for smooth surface and 9.743 for rough surfaces
F_j	mass flux at face j
G	generation of k in equation (3.16)
H_1, H_2	channel width downstream and upstream of the step
H	width of a channel in figure(4.1) and step height in figure(4
l_0	length scale of turbulence
k	turbulent kinetic energy
k^+	nondimensionalised turbulent kinetic energy $\frac{k}{u_\tau^2}$
L_s	step length
$\bar{P}$	time averaged pressure
p'	pressure correction in equation (2.32)
Re_L	Reynolds number based on charecteristic length L
S_u	source term for u momentum equation
S_w	source term for w momentum equation
S_u	source term for v momentum equation
S_k	source term for k momentum equation
S_ϵ	source term for ϵ momentum equation
S_j	surface area of face j
$\bar{u}, \bar{w}, \bar{v}$	time averaged velocites in cartesian coordinates
$\bar{U}, \bar{W}, \bar{V}$	nondimensional time averaged velocites
U_0	reference velocity
u', v', w'	correction for u, v, w velocities in equation(2.25)
U_τ	nondimensional frictional velocity
U^+	nondimensionalised velocity with respect to friction

	velocity($\frac{U}{U_\tau}$)
x, y, z	cartesian coordinates
X, Y, Z	nondimensional cartesian coordinates
X_R	nondimensional reaatachment length
y^+	dimensionless distance $\frac{u_\tau y}{\nu}$

Greek Symbols

ϕ	any scalar or vector quantity
ρ	density of a fluid
ϵ	dissipation rate of turbulent kinetic energy
ν	kinematic viscosity
ν_t	turbulent viscosity
$\nu_{t,n}$	nondimensionalised turbulent viscosity $\frac{\nu_t}{\nu}$
μ	dynamic viscosity
τ_w	wall shear stress
$\sigma_k, \sigma_\epsilon$	turbulent Prandtl number for k and ϵ in equation (3.16) and (3.17)
$\alpha_1, \alpha_2, \alpha_3$	coefficients of unit vectors in equation (2.18)
χ	von Karman constant
λ	constant in equation (3.28)
Γ_ϕ	constant or variable coeeficient in equation (2.17)

Subscripts

i, j, k	tensor notations
t	turbulence value
P	finite volume cell location

Chapter 1

Introduction

During the early days of the computational fluid dynamics(CFD) finite-difference methods see e.g Patankar[1] were the most popular. They are algorithimically simple, efficient, and accurate. However they are best used on uniform grids and hence in regular computational domains. However, with the advancement of C.F.D and its application to industrial problems there is a need for methods for computing flows in complex geometries. To adapt the finite difference method for complex geometries, we can map the complex domain onto simple domains and solve the problems there. This requires that the governing equations be represented using generalised curvilinear co-ordinates this makes the Partial differential equation quite complicated and leads to a loss of computational efficiency and accuracy. Alternatively one can use schemes based on the Finite element or Finite volume methods.

Finite element methods have been increasingly applied to CFD see e.g Hughes[2]. They can be applied to complex flow domains. However these methods though very powerful are not simple to implement and their computational efficiency vis-a-vis the finite difference method is doubtful

An alternate development is that of the finite volume methods see e.g. Hirsch[3] which are essentially a generalisation of the finite difference method but uses the integral form of the governing equations of flow, rather than their differential form. This gives greater flexibilty in handling complex domains as the finite volumes need not be regular(rectangular) shaped. This approach, too, has some problems the staggered grid with non-coinciding pressure and velocity grid points, traditionally used to by finite difference solver to avoid numerical pressure-velocity decoupling are difficult, and computationally expensive, to use in complex finite volume codes. Thus the use of the non-staggered or collocated grid, with the same locations for pressure and velocity grid-points is becoming popular.

The simplest approach to tackle complex domains is to use an orthogonal grid but make modifications on the boundary to accomodate the irregularity. The advantage of this is that orthogonal grids are used, but with the disadvantage that the boundaries are only approximately represented. Orthogonal grids have often been used for solving the flow equations for a complex geometry. Pope[4] applied the conservative forms of the equations with the finite volume method for simulating turbulent flow in diffusers. Rapley[5] also used orthogonal grids for calculation of turbulent flows. The calculations in entrance region of a chanel with an arbitrary shaped cross section were performed by Whitlaw *et. al.*[6].

A general curvilinear co-ordinates are usually used along with non-orthogonal body-fitted grids which exactly coincide with the boundaries of the complex physical domain. The governing partial differential equations transformed in terms of these curvilinear co-ordinates are then solved. The successful use of this method was made among others by Galchen and Somerville[7] and Faghri *et. al.*[8]. Faghri[8] used algebraic co-ordinate transformation. Acharya and Patankar[9] used an adaptive grid procedure for parabolic flow problems for irregular geometries. All these methods employed staggered grids. The suc-

cessful application of finite volume method using a collocated i.e non-staggered, grid was made by Hsu[10],Rhie[11],Peric[12] and others. Hsu[10] and Peric[12] solved the equations on a physical domain thus avoiding the need for transformation,while Rhie mapped the non-orthogonal grid onto a rectangular mesh on which the transformed equations were solved. Mukhopadhay *et. al.*[13] used the staggared grid for the solution of equations on the physical domain without transformtion. Verma and Eswaran[14] have developed a Finite volume approach directly applied on the physical domain. Satya prakash *et. al.*[15] developed a transient Navier-Stokes algorithm using finite volume method employing a collocated grid for complex geometries, in which the equations are solved in a physial domain.

1.1   k-ε modelling of turbulent flows

The numerical solution of the transient Navier-Stokes equations for turbulent flows without turbulence modelling , but with sufficient accuracy and resolution to capture turbulence behaviour, are called Direct Numerical Simulations(DNS) of turbulence. Direct Numerical Simulation, although an unsurpassed method for understanding the physics of turbulent flow can be currently used only for Reynolds number less than 10^3 due to constraints of computer memory and speed. Practical needs of industry demands numerical solutions for high Reynolds number(10^6) flow problems.

An alternative to Direct Numerical Simulation is to use the Reynolds Averaged Navier-Stokes equations. In this approach, the statistical average of the Navier Stokes equations are used as governing equations to describe the mean quantities. However, the averaged equations no longer constitute a closed system of equations. The system can be closed only with the aid of semi-emperical models. Averaging gives rise to extra stress terms called

Reynold stresses, which have to be so modelled.

Usually in turbulence modelling, the Reynolds stress terms are approximated using a Boussinesq eddy viscosity concept which assumes that, in analogy to the viscous stresses in laminar flows, the turbulent stresses are proportional to the mean velocity gradient. The whole purpose of the modelling then becomes the prediction of the *eddy viscosity* which substitute the kinematic viscosity of the Navier-Stokes equation. The simplest model for eddy viscosity is the Constant Eddy Viscosity model which however has few successful applications. Another method is to specify an algebraic relationship for eddy viscosity as in e.g., the Prandtl *mixing length* model. Such models are called *Zero equation* models because no additional partial differential equations are needed to be solved to implement the model.

One equation models specify the eddy viscosity by an emperical relationship with turbulent kinetic energy and a charecteristic length-scale. The turbulent kinetic energy is computed using a partial differential equation and the length-scale is specified algebraicaly.

The most succesful popular model ,however, k-ϵ model which is a two equation model that uses transport equations for k and ϵ and with these two equations obtaine the eddy viscosity. The k-ϵ model contains five constants which are not truly universal and thus varies according to the flow situation. Rodi[16] lists several cases where the k-ϵ model has been successfully applied using given model constants values.

Some of the difficulties of k-ϵ model are.

1. The k-ϵ model uses a Boussinesq eddy viscosity concept which assumes that turbulent viscosity is isotropic. Therefore it cannot reproduce secondary flows which arise due to unequal normal Reynolds stresses.

2. Boussinesq eddy viscocity concept cannot accurately simulate the effect, on turbulence, of the changes in the mean flow direction across the shear layers.

3. The turbulence production in highly strained flows is over-predicted by the k-ϵ model.

4. The k-ϵ model requires modification when applied to flows with highly curved stream lines.

5. The k-ϵ model does not strictly satisfy the realizability constraint.($\tau_{ij} > 0$) .

A variety of modified version's of the k-ϵ model have been used to improve its performance, among which are the RNG k-ϵ model of Yakhot *et. al.*[17] and the Non-linear k -ϵ model of Speziale[18]. Some Low Reynolds number form of k -ϵ model have been developed which use damping functions to damp the turbulence near a solid wall surface due to molecular viscosity. Many such model's appeared with different constants & damping function's the comparison of which is given in Patel[19].

1.2 Development of Finite Volume Code for complex 3-D geometries

A Finite Volume Code to solve laminar Navier-Stokes equations has been developed by Satya Prakash *et. al.*[15]. The code has been tested on different regular geometries like 1)Lid driven 2-D and 3-D cavity flow. 2)Channel flow 3)Sudden expansion in a channel. The results in these studies are in good agrrement with published results.

This code uses an explicit transient algorithm by which both steady and

unsteady flows can be solved. The Navier-Stokes equations are solved on a non-staggered, and possibly non-orthogonal, grid . A special(*momentum*) interpolation technique is used to avoid the decoupling of pressure from the velocity field in the numerical solutions. An implicit time stepping version has also been developed. Efforts are in progress for testing this code on a cylindrical and irregular geometries.

In this work presented here we incorporate the standard linear k-ϵ model of Launder *et. al.*[20] with wall function approach of Launder and Spalding[21] for simulation of turbulent flows in the above solver. The extended code is then tested on channel flow and flow over a backward facing step. results.

Chapter 2

Finite - Volume Formulation

In this chapter we describe the finite-volume formulation used in the DRDL code (Satya Prakash *et al*[15]). The formulation included only the Navier-Stokes and continuity equation. The $k - \epsilon$ model has been incorporated as part of this thesis work.

2.1 Governing Equations

The three-dimensional Reynolds-averaged Navier-Stokes equations for incompressible turbulent flow for an arbitrary spatial region of control volume V bounded by a closed surface S can be expressed in the following general convection-diffusion-source integral form:

$$\int_S \mathbf{u} \cdot \mathbf{dS} = 0 \qquad (2.1)$$

$$\frac{\partial}{\partial t} \int_V \phi dV + \int_S [\mathbf{u}\phi - \frac{\Gamma_\phi}{\rho} \nabla\phi] \cdot \mathbf{dS} = \frac{1}{\rho} \int_V S_\phi dV \qquad (2.2)$$

where ρ is the fluid density, $\mathbf{u}$ is the mean fluid velocity with components u, v, w, ϕ stands for any vector component or scalar quantity, S_ϕ is the volumetric source term. The various source terms are.

$$S_u = -\frac{1}{\rho}\frac{\partial p}{\partial x} + \frac{\partial}{\partial x}(\nu_t \frac{\partial u}{\partial x}) + \frac{\partial}{\partial y}(\nu_t \frac{\partial v}{\partial x}) + \frac{\partial}{\partial z}(\nu_t \frac{\partial w}{\partial x}) \qquad (2.3)$$

$$S_v = -\frac{1}{\rho}\frac{\partial p}{\partial y} + \frac{\partial}{\partial x}(\nu_t \frac{\partial u}{\partial y}) + \frac{\partial}{\partial y}(\nu_t \frac{\partial v}{\partial y}) + \frac{\partial}{\partial z}(\nu_t \frac{\partial w}{\partial y}) \qquad (2.4)$$

$$S_w = -\frac{1}{\rho}\frac{\partial p}{\partial z} + \frac{\partial}{\partial x}(\nu_t \frac{\partial u}{\partial z}) + \frac{\partial}{\partial y}(\nu_t \frac{\partial v}{\partial z}) + \frac{\partial}{\partial z}(\nu_t \frac{\partial w}{\partial z}) \qquad (2.5)$$

$$S_k = G - \epsilon \qquad (2.6)$$

$$S_\epsilon = C_{1\epsilon}\frac{\epsilon}{k}G - C_{2\epsilon}\frac{\epsilon^2}{k} \qquad (2.7)$$

In this formulation we work with **cartesian components** of velocity. So ϕ can be the three cartesian components of velocity u, v, w, as well as any scalar e.g., k, or ϵ which needs to be determined. The last two source terms correspond to the equations for kinetic energy k ,and the turbulent energy dissipation ϵ,from the $k - \epsilon$ model,$C_{1\epsilon}$ and $C_{2\epsilon}$ are model constants and G is the generation term which shall be explained later.

2.2   Description of the Finite-Volume

Figure 2.1 shows the kind of control volume used, with eight vertices but otherwise irregular.

The conservation equations are discretized by employing the general finite-volume approach. The solution domain is subdivided into a number of contiguous (finite) control volumes. The control volumes are defined by the coordinates of their vertices which are assumed to be connected by straight lines. The coordinates of the control volume vertices are calculated by some grid generation procedure. A **Collocated Grid** arrangement is employed, i.e., all the dependent variables $(u, v, w, p, k, \epsilon)$ are defined at the same location, the centroid of the control volume in Figure 1. The six neighbouring control volume centers are indicated by E, W, N, S, T, and B (for the east, west, north,
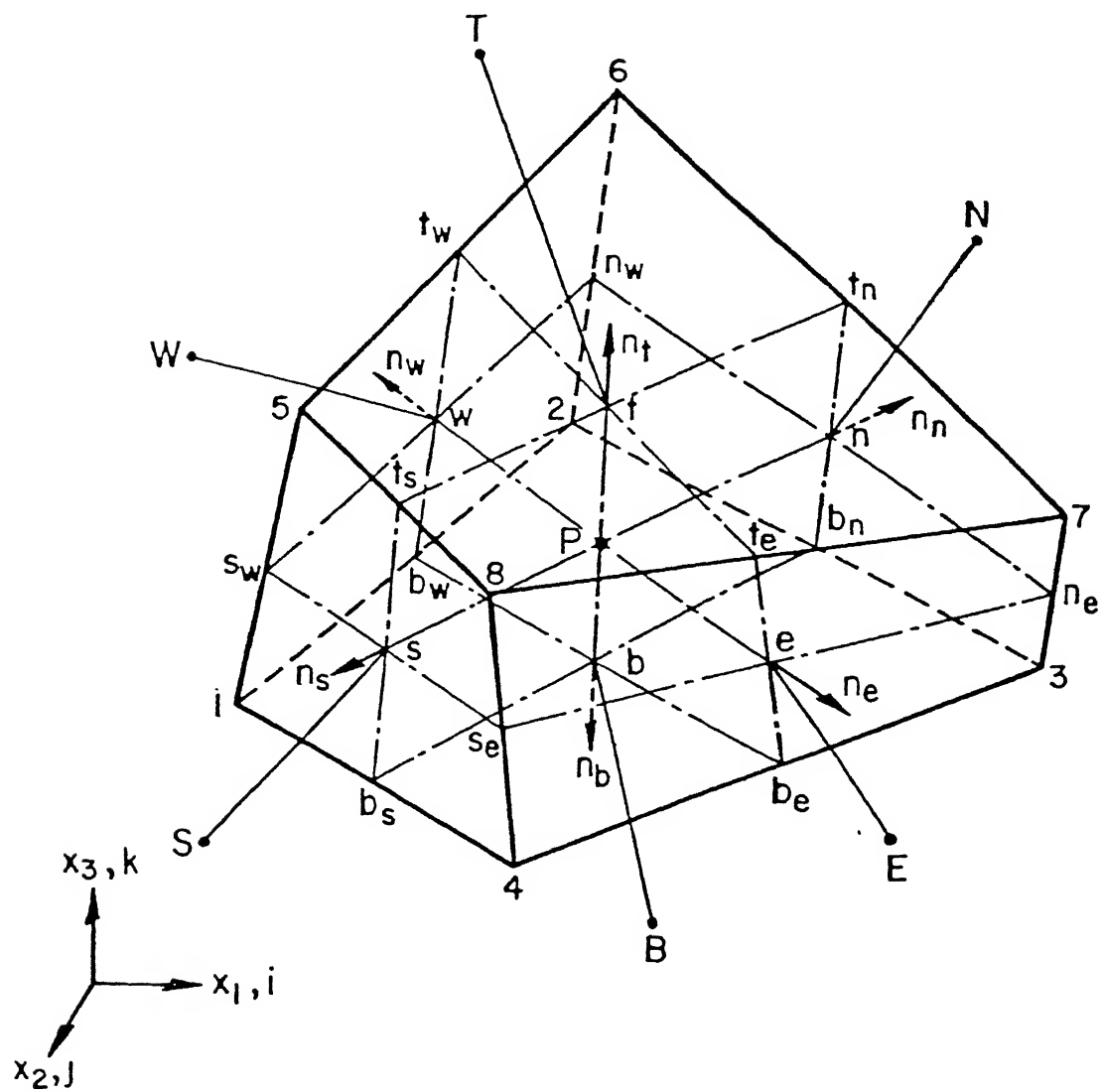
Figure 2.1: Three Dimensional control volume

south, top and bottom neighbours). The face center points e, w, n, s, t, and b are located at the corresponding face centroids of control volume P. Note the edge-centers te, be, ne, se, etc. which are also needed in the computations.

Before the time-stepping can proceed all geometrical parameters need to be computed as part of the initialization. These parameters include the surface vectors for each of the six faces e, w, n, s, t, b of each finite volume and also its volume. These computations can be done by the methods suugested by Kordulla and Vinokur[22] and the details of the application can be found in reference 15.

2.3   Discretization Procedure

All the conservation equations have the same general form, represented by

$$\frac{\partial}{\partial t} \int_V \rho\phi dV + \int_S [\rho\mathbf{u}\phi - \Gamma_\phi \nabla\phi] \cdot \mathbf{dS} = \int_V S_\phi dV \qquad (2.8)$$

The main steps of the discretization procedure to calculate convection and diffusion fluxes and source terms are outlined below. The rate of change and source terms are integrated over the cell volume, whereas the convection and diffusion terms form the sum of fluxes through the CV faces.

2.3.0.1   Continuity Equation

Equation (2.1) is discretized in the following way.

$$\int_S \rho\mathbf{u} \cdot \mathbf{dS} \Rightarrow \sum_{j=e,w,n,s,t,b} \rho(\mathbf{u} \cdot \mathbf{S})_j \qquad (2.9)$$

where $\mathbf{S}_j$ is the surface vector representing the area of the jth cell face and $\mathbf{u}_j$ is the velocity defined at the face center j.

In discretized form the continuity equation follows

$$\sum_j F_j = F_e + F_w + F_n + F_s + F_t + F_b = 0 \qquad (2.10)$$

where the F_j is the outward mass flux through face j, defined by

$$F_j = \rho \mathbf{u}_j \cdot \mathbf{S}_j$$

2.3.0.2 Discretization of General Convection-Diffusion Equation

(a) Rate of change

The value of the dependent variable ϕ at the centroid of the control volume (the geometric center) represents an average over the CV as a whole. Thus, using forward difference time-stepping we get:

$$\frac{\partial}{\partial t} \int_V \rho \phi dV \Rightarrow \rho V \frac{\phi_P^{n+1} - \phi_P^n}{\Delta t} \qquad (2.11)$$

where V is the volume of the cell.

(b) Convection fluxes

The surface integral of the convection flux of variable ϕ is approximated in the following way.

$$\int_S \rho \mathbf{u} \phi \cdot d\mathbf{S} \; \Rightarrow \; \sum_j \rho \phi_j (\mathbf{u} \cdot \mathbf{S})_j \qquad (2.12)$$
$$= \; \sum_j F_j \phi_j$$

where ϕ_j is the value of ϕ at the center of face j. Thus

$$\int_S \rho \mathbf{u} \phi . d\mathbf{S} \Rightarrow F_e \phi_e + F_w \phi_w + F_n \phi_n + F_s \phi_s + F_t \phi_t + F_b \phi_b \qquad (2.13)$$

where ϕ_e is the (interpolated) value of the variable ϕ at the east face center, etc. This is evaluated by using a *weighted upwind* interpolation between the neighbouring nodal values, say ϕ_P and ϕ_E. This weighted upwind methods

takes weighted average of the centre-difference (linear interpolation) between ϕ_P and ϕ_E and the first order upwind approximation.

$$\phi_e^{UDS} = \begin{cases} \phi_P & if\ F_e \geq 0 \\ \phi_E & otherwise \end{cases} \tag{2.14}$$

The centre-difference approximation is

$$\phi^{CDS} = \frac{V_E \phi_P}{V_E + V_P} + \frac{V_P \phi_E}{V_E + V_P} \tag{2.15}$$

where V_E and V_P are the volumes of the cells E and P respaectively. Here cell volumes are used for interpolation, instead of cell dimensions, so as to handle irregular finite-volumes if necessary. In the weighted upwind discretization the convection flux is split into the first-order upwind differencing approximation, and another part, which equals the difference between the central difference scheme (CDS) and UDS approximations:

$$F_e \phi_e = (F_e \phi_e)^{UDS} + \gamma[(F_e \phi_e)^{CDS} - (F_e \phi_e)^{UDS}],\ \text{etc} \tag{2.16}$$

Multipliccation of the second part by a factor $\gamma(0 \leq \gamma \leq 1)$ allows the introduction of numerical diffusion. ($\gamma = 0$ means pure UDS, $\gamma = 1$ means pure CDS).The lower value of the γ enhance the numerical stability of the solution algorithm, but at the cost of accuracy. In practice one should use the highiest value of $\gamma \leq 1$, which allows numerical stability. This optimum value of the γ depends upon the grid peclet number of the computations. If a fully implicit method is used for time-stepping, the upwind parts of the equation(2.16) are 'implicit' in that they are incorporated in the coefficients of the unknown velocity during the pressure-velocity iterations. The CDS terms on the other hand are evaluated using previous iteration values and used as source term on the right hand side of the same equation. This is the so-called *deferred correction* approach of Khosla and Rubin[23] which has been incorporated in the implicit code(reference 15).

(c) Diffusion fluxes

The diffusion flux of variable ϕ through the cell faces is evaluated as given in reference 15.

$$\int_S \Gamma_\phi \nabla \phi \cdot \mathbf{dS} \approx \sum_{j=e,w,n,s,t,b} (\Gamma_\phi \nabla \phi \cdot \mathbf{S})_j \equiv \sum_j -F_j^d \qquad (2.17)$$

where any face S_j can be expressed as

$$\mathbf{S}_j = \alpha_1 \mathbf{n}^1 + \alpha_2 \mathbf{n}^2 + \alpha_3 \mathbf{n}^3 \qquad (2.18)$$

where $\mathbf{n}^1$, $\mathbf{n}^2$ and $\mathbf{n}^3$ are any three linearly independent (not necessarily orthogonal) unit vectors. The details of the calculations of $\alpha_1, \alpha_2, \alpha_3$ which depends on the local grid perticulars can be found in Satya Prakash *et. al.* [15].

The diffusion flux is made of two distinct parts: normal diffusion and cross-derivative diffusion. The second part arises from the nonorthogonality of the grid. The normal derivative diffusion flux approximation of ϕ through any cell face involves the values of ϕ, at cell centres whereas the cross-derivative diffusion flux approximation takes into account the edge center values of ϕ. (The normal derivative diffusion flux is treated implicitly in implicit time-stepping while the cross-derivative diffusion flux is treated explicitly to avoid the possibility of producing negative coefficients in an implicit treatment). The diffusion flux at any face of the cell, say east, is given by.

$$F_e^d = -\Gamma_\phi (\alpha_1 \frac{\phi_E - \phi_P}{\Delta x^1} + \alpha_2 \frac{\phi_{se} - \phi_{ne}}{\Delta x^2} + \alpha_3 \frac{\phi_{te} - \phi_{be}}{\Delta x^3}) \qquad (2.19)$$

The edge center values appearing in cross-derivative diffusion flux are calculated by using the linear interpolation (Satya Prakash *et. al.* [15]).

(d) Sources

The source term is integrated over the cell volume. By assuming that the value at the CV center represents the mean value over the whole control volume, we can write

$$\int_V S_\phi dV \Rightarrow (S_\phi)_P V \qquad (2.20)$$

Apart from the real source S_ϕ, explicitly treated parts of the convection and diffusion fluxes are added to S_ϕ.

The pressure term in momentum equation is treated explicitly in the *predicted* step(see below). Its discretization for the ith momentum equation is

$$-\int_S pn_i \mathbf{S} \Rightarrow -\sum_j p_j S_{ij}$$

where p_j is the pressure at the jth face center and S_{ij} is the ith component of the surface vector for face j.

2.4   Semi-Explicit Time Stepping

We use an explicit time-stepping algorithm for the scalars k, ϵ (and any others we may want to compute later temperature etc.). That is every term for the convection,diffusion and source are evaluated using current known values at next time step 'n' to compute the values at the next time step, explicitly, as this unknown value appears only once in the time-derivative. This simple approach cannot be adopted for the momentum equations because the pressure and the velocity components are simultaneously unknown. The pressure has to be such that the continuity equation is satisfied, but there is no seperate equation for pressure. Thus iteration is inevitable and the approach adopted is semi-explicit-i.e. the convective,diffusive and source terms are treated explicitly i.e. evaluated at 'n' time level, but the pressure is treated as unknown.

For the present situation we will adopt a semi-implicit scheme in which the three momentum equations

$$\rho V \frac{u_P^{n+1} - u_P^n}{\Delta t} + \sum_j (F^c + F^d)^n = -\sum_j p_j^{n+1} S_{ij} \qquad (2.21)$$

where u is the ith component of velocity, have to be solved along with

$$\sum_j F_j^{n+1} = 0 \qquad (2.22)$$

for each finite volume cell. We adopt a two step process. First a predicted velocity $u^\star$ is found which satisfies the equation

$$\rho V \frac{u_P^\star - u_P^n}{\Delta t} + \sum_j (F^c + F^d)^n = -\sum_j p_j^n S_{ij} \qquad (2.23)$$

Subtracting equation (2.23) from (2.21) we get

$$\rho V \frac{u_P'}{\Delta t} = -\sum_j p_j' S_{ij} \qquad (2.24)$$

where the corrections

$$u_P' = u_P^{n+1} - u_P^n \qquad p_j' = p_j^{n+1} - p_j^n \qquad (2.25)$$

and the corresponding flux corrections F_j' have to satisfy

$$\sum_j F_j' = -\sum_j F_j^\star \qquad (2.26)$$

In the *predictor* step, the predicted velocity is computed using(2.23),and in the corrector step(2.24) and (2.26) are treated till convergence is achieved and and the correction of pressure and velocity are added to the predicted values to obtain the final values for that time-step.

$$\mathbf{u}^{n+1} = \mathbf{u}^\star + \mathbf{u}' \qquad (2.27)$$

$$p^{n+1} = p^n + p' \qquad (2.28)$$

Due to the non-staggered variable arrangement, if the variables (velocities and pressure) at the cell faces are calculated by linear interpolation between the adjacent cell centered quantities then the pressure-velocity iterations do not converge and lead to a *checker board* pressure field. Therefore it is important to use *momentum interpolation*(Hirsh*et. al.*[24] in which the velocity at the cell faces are computed by allowing linear interpolation of the convective and diffusive terms but not of the pressure term.

2.5   Solution Algorithm

The velocity and pressure fields are calculated with the following Gauss-Seidel type algorithm:

1. Use equation (2.23) to compute the cell-center $\mathbf{u}_P$ and $\mathbf{v}_P$. Make an initial guess p_P. Use interpolation to obtain the face-center quantities $\mathbf{v}_j$ and p_j.

2. Compute the mass flux through each cell face j using

$$F_j^\star = \rho \mathbf{v}_j \cdot \mathbf{S}_j - \Delta t \nabla p_j \cdot \mathbf{S}_j \qquad (2.29)$$

3. Use equation $\mathbf{u}_j' = -\frac{\Delta t}{\rho} \nabla p_j'$ to compute the flux correction at the face j,

$$F_j' = -\Delta t \nabla p_j' \cdot \mathbf{S}_j \qquad (2.30)$$

   This is computed using the formulation for diffusion fluxes by replacing ϕ by p'.

4. Compute residual for each cell,

$$\Re = -\sum_j F_j^\star - \sum_j F_j' \qquad (2.31)$$

5. Calculate the cell-center pressure correction from the relation

$$p_P' = p_P' + \omega \frac{\Re}{a_P} \qquad (2.32)$$

   where ω is relaxation factor and a_P stands for diagonal coefficients that is calculated from

$$a_P = -\Delta t \left[\frac{\alpha_1}{\Delta x^1}\Big|_w - \frac{\alpha_1}{\Delta x^1}\Big|_e + \frac{\alpha_2}{\Delta x^2}\Big|_n - \frac{\alpha_2}{\Delta x^2}\Big|_s + \frac{\alpha_3}{\Delta x^3}\Big|_b - \frac{\alpha_3}{\Delta x^3}\Big|_t \right]$$
$$(2.33)$$

   where α_1, α_2, etc. are the same as in p' gradient calculations above.

6. If $\Re_{rms} > \epsilon$ goto step 3

7. Store the updated mass flux through cell-faces from

$$F_j^\star = F_j^\star - \Delta t \nabla p_j' \cdot \mathbf{S}_j \qquad (2.34)$$

8. Store the updated pressure at cell-center $p_P = p_P + p_P'$

9. Store the cell-center corrected velocity

$$\mathbf{u}_P' \;\; = \;\; -\frac{\Delta t}{\rho V_P} \sum_j p_j' S_{ij}, \qquad (2.35)$$

$$\mathbf{u}_P \;\; = \;\; \mathbf{u}_P + \mathbf{u}_P' \qquad (2.36)$$

10. Calculate the turbulent viscosity by solving the k and ϵ equation.

11. Goto step 1 and repeat the process until steady state is reached.

Chapter 3

$k - \epsilon$ Modelling

The continuity equation and the Navier-Stokes equation, with the associated boundary conditions, completely describe the behaviour of a Newtonian viscous fluid flow. For an incompressible fluid, the governing equations are continuity equation

$$\frac{\partial u_i}{\partial x_i} = 0, \tag{3.1}$$

and the Navier-Stokes equation

$$\frac{\partial u_i}{\partial t} + u_j \frac{\partial u_i}{\partial x_j} = -\frac{1}{\rho} \frac{\partial p}{\partial x_i} + \nu \frac{\partial^2 u_i}{\partial x_j \partial x_j}, \tag{3.2}$$

where u_i is the instantaneous velocity component in the x_i direction, p is the pressure, ρ is the density, ν is the kinematic viscosity, and the Einstein summation convention applies to the repeated indices (i and j take a value of 1 to 3). Although they are used mainly to solve laminar flows, equation(3.1) and (3.2) are valid for any Reynolds number, i.e., even for turbulent flows, but in this case the solution fluctuates so rapidly, and at such small scales, that it is extremely difficult to obtain an accurate numerical solution.

However such solutions (called Direct Numerical Simulations) of the above two equations can be attempted for turbulent flows, but the difficulty is that the capacity of the present computers does not allow the DNS to be used for high Re flows. Also engineers are usually not as interested in the fluctuating velocity of turbulence as in the mean flow behaviour. Therefore a statistical approach is usually taken. This approach usually involves the Reynolds Averaged Navier-Stokes equations.

3.1   Reynolds Averaged Navier-Stokes equation

To obtain these equations, a *time* average is taken of the Navier-Stokes and continuity equation. Velocities and pressure fluctuation are decomposed into mean and fluctuating quantities

$$u_i = \bar{u} + u_i^{'} \, , \, p = \bar{p} + p^{'} \tag{3.3}$$

in which the overbar denotes the mean quantity and the prime denotes the fluctuating part. The mean quantites, $\bar{u}_i$ and $\bar{p}$ are defined as

$$\bar{u}_i = \frac{1}{T} \int_{t_0}^{t_0+T} u_i \, dt, \quad \bar{p}_i = \frac{1}{T} \int_{t_0}^{t_0+T} p \, dt \tag{3.4}$$

where t_0 is any arbitrary time and T is a time scale larger than the largest time scale of turbulence. During averaging the following rules are valid

$$\begin{aligned} \bar{u_i^{'}} &= 0 \, , \, \bar{p^{'}} = 0 \\ \overline{u_i u_j} &= \bar{u}_i \bar{u}_j + \overline{u_i^{'} u_j^{'}} \\ \overline{u_i^{'} \bar{u}_j} &= \overline{u_j^{'} \bar{u}_i} = 0 \end{aligned} \tag{3.5}$$

The averaging then leads to

$$\frac{\partial \bar{u}_i}{\partial x_j} = 0 \tag{3.6}$$

$$\frac{\partial \bar{u}_i}{\partial t} + \bar{u}_j \frac{\partial \bar{u}_i}{\partial x_j} = -\frac{1}{\rho} \frac{\partial \bar{p}}{\partial x_i} + \frac{\partial}{\partial x_j} (\nu \frac{\partial \bar{u}_i}{\partial x_j} - \overline{u_i^{'} u_j^{'}}) \tag{3.7}$$

The equations for the average quantities are very similar to the equations (3.1) and (3.2) for the instantaneous velocity and pressure fields. The extra terms $(\overline{u_i' u_j'})$ in the above equation, in comparison to equation (3.2) arise due to averaging of the nonlinear convective terms $(u \cdot \nabla u)$ in the momentum equation and are known as Reynolds stresses. These terms form a symmetric tensor, and are often called stresses because they correspond to the retarding effect due to turbulent transport of momentum.

3.2 Boussinesq Approximation

The Reynolds-stress tensor (for incompressible flows) is often modelled by the widely-used *Boussinesq* approximation in most present day turbulence models. This approximation involves the so-called *Eddy-Viscosity* concept, and is based on an analogy with the viscous stresses in laminar flows, the turbulent stresses are also assumed to be proportional to the mean velocity gradients in the following way

$$\overline{u_i' u_j'} = -\nu_t \left(\frac{\partial \bar{u}_i}{\partial x_j} + \frac{\partial \bar{u}_i}{\partial x_i} \right) + \frac{2}{3} k \delta_{ij}, \qquad (3.8)$$

in which ν_t is the turbulent or eddy-viscosity. This eddy viscosity ν_t is not a fliud property, like the molecular viscosity ν, but is a function of the turbulent velocity field. In analogy to the kinetic theory of gases, the turbulent viscosity may be expressed as

$$\nu_t \propto v_0 l_0 \ \text{ or } \ \nu_t \propto l_0^2 / \tau_0 \qquad (3.9)$$

in which v_0 is the relevant velocity scale, l_0 is the length scale and τ_0 is the time scale of turbulence. However, it is well known that the turbulent flows contains a wide range of length and time scales and so there is an inherent limitation to the applicability of the eddy viscosity concept. There are also other reasons why this concept is criticised, (see, e.g, Biswas and Eswaran[25]).

Inspite of these limitations, this concept is very widely used in turbulence

models today. Its great advantage lies in that the problem of modelling the six independent quantities, $\overline{u_i'u_j'}$, is replaced by the problem of modelling the single quantity ν_t, the eddy-viscosity. Thus specification of the eddy-viscosity constitutes the core of the majority of the turbulence models for engineering applications. These models are discussed in the next section.

3.3   Types Of Turbulence Models

The following models all assume the Boussinesq approximation(3.8). They differ only in the method used to estimate the eddy-viscosity, ν_t.

3.3.1   Zero-Equation Models

These are the simplest among the turbulence models. They do not employ the use of any extra transport equation for, say, the turbulent kinetic energy or some other quantity, for the purpose of modelling.

Two of the commonly used Zero-equation models are

(a) Constant Eddy Viscosity Models:

In these models, ν_t is specified as a constant and its value is chosen depending on some experimental information and or by trial and error procedure . These models are obsolete.

(b) Mixing Length Models:

This model was propsed by Prandtl. He postulated that

1. the turbulent length scale, l_0 is equal to the mixing length, l_m and

2. the velocity scale, v_0 is equal to the mean velocity gradient times the mixing length.

when these assumptions are substituted into equation (3.9) we get

$$\nu_t = l_m^2 \left| \frac{\partial \bar{u}}{\partial y} \right| \tag{3.10}$$

where the constants of proportionality has been assumed to be unity. This model is closed once the mixing length, l_m is specified by some simple emperical formulation.

3.3.2   One-Equation Models

In these models, the velocity scale, v_0 of the turbulence is taken as $\sqrt{k}$, where k is the turbulent kinetic energy $k = \frac{3}{2}\overline{u_i' u_i'}$. The eddy viscosity then can be written as.

$$\nu_t = \sqrt{k} l_0 \tag{3.11}$$

In one-equation models, l_0 is specified emperically while the turbulence kinetic energy is determined by solving the model equation:

$$\frac{\partial k}{\partial t} + \bar{u}_j \frac{\partial k}{\partial x_j} = \nu_t \left[\frac{\partial \bar{u}_i}{\partial x_j} + \frac{\partial \bar{u}_j}{\partial x_i} \right] \frac{\partial \bar{u}_i}{\partial x_j} + \frac{\partial}{\partial x_j} \left[\frac{\nu_t}{\sigma_k} \frac{\partial k}{\partial x_j} \right] - C_D \frac{k^{3/2}}{l_0} + \nu \nabla^2 k \tag{3.12}$$

in which σ_k and C_D are emperical constants. For simple flows, the suggested value of σ_k and C_D are 1.0 and 0.08 respectively.

3.3.3   Two-Equation Models

Two-equation models are among the most popular for scientific and engineering calculations. In these models, two separate transport equations are solved to determine the length and velocity scales for the eddy viscosity.

The transport equation for the velocity scale in the two-equation models is usually the k equation [equation(3.12)] as given for the one equation models. However, the other transport equation need not necessarily have the length

scale itself as the dependent variable - any combination of k and l_0 may be used as the dependent variable in the second transport equation. Kolmogorov proposed a transport equation for the frequency $\sqrt{k}/l_0$, Rotta proposed an equation kl_0, while Spalding suggested a transport equation for the vorticity , k/l_0^2. The $k - \epsilon$ uses a transport equation for the turbulent dissipation rate, ϵ.

The transport equation for any of the above quantities can be expressed in the general form:

$$\frac{\partial z}{\partial t} + \bar{u}_j \frac{\partial z}{\partial x_j} = \frac{\partial}{\partial x_j} \left(\frac{\sqrt{k}l_0}{\sigma_z} \frac{\partial z}{\partial x_j} \right) + C_{z1} \frac{z}{k} G - C_{z2} z \frac{\sqrt{k}}{l_0} + S \quad (3.13)$$

in which, $z = k^m l_0^n$, G is the production term of z, $S =$ is a secondary source term which depends on choice of z, and σ_z, σ_{z1} and σ_{z2} are emperical constants. Past experience indicates that the $k - \epsilon$ model works better than the other two-equation models based on equation (3.13). The description of the $k - \epsilon$ model is presented in the next section.

3.4 $k - \epsilon$ Model

The length and time scales in this model are obtained from the turbulent kinetic energy, k, and the turbulent dissipation rate, ϵ, using the dimensional arguments

$$l_0 \propto \frac{k\sqrt{k}}{\epsilon} \text{ and } \tau_0 \propto \frac{k}{\epsilon} \ ; \quad (3.14)$$

substitution in equation (3.9) gives

$$\nu_t = C_\mu \frac{k^2}{\epsilon} \quad (3.15)$$

in which C_μ is an emperical constant. The turbulent kinetic energy and the dissipation rate are obtained by solving their respective modeled transport equations. The transport equations for k in the $k - \epsilon$ model require modeling of only the turbulent transport term whch is done using the gradient

approximation. This is given as

$$
\overbrace{\frac{\partial k}{\partial t} + \overbrace{\bar{u}_j \frac{\partial k}{\partial x_j}}^{\text{convection}}} = \nu_t \overbrace{\left[\frac{\partial \bar{u}_i}{\partial x_j} + \frac{\partial \bar{u}_j}{\partial x_i}\right]\frac{\partial \bar{u}_i}{\partial x_j}}^{\text{production}} + \overbrace{\frac{\partial}{\partial x_j}\left(\frac{\nu_t}{\sigma_k}\frac{\partial k}{\partial x_j}\right)}^{\text{turbulent diffusion}}
$$

$$
- \overbrace{\epsilon}^{\text{dissipation of k}} + \overbrace{\nu \nabla^2 k}^{\text{molecular diffusion}} \qquad (3.16)
$$

The transport equation for ϵ is

$$
\frac{\partial \epsilon}{\partial t} + \overbrace{\bar{u}_j \frac{\partial \epsilon}{\partial x_j}}^{\text{convection}} = \overbrace{\nu \nabla^2 \epsilon}^{\text{molecular diffusion}} + \overbrace{\frac{\partial}{\partial x_j}\left(\frac{\nu_t}{\sigma_\epsilon}\frac{\partial \epsilon}{\partial x_j}\right)}^{\text{turbulent diffusion of } \epsilon} +
$$

$$
\overbrace{C_{\epsilon 1}\frac{\epsilon}{k}\left(\frac{\partial \bar{u}_i}{\partial x_j} + \frac{\partial \bar{u}_j}{\partial x_i}\right)\frac{\partial \bar{u}_j}{\partial x_j}}^{\text{production}} - \overbrace{C_{\epsilon 2}\frac{\epsilon^2}{k}}^{\text{dissiaption}} \qquad (3.17)
$$

Speziale showed that the modelling of the producition term in the ϵ equation is strictly valid only when

1. there is a clear separation in the time scale of turbulent fluctuation and the mean velocity field and

2. the level of anisotropy is not very much

We use the constant values given by Launder and Spalding[21] $C_{\epsilon 1} = 1.44$, $C_{\epsilon 2} = 1.92$, $\sigma_k = 1.0$, $\sigma_\epsilon = 1.30$ and $C_\mu = 0.09$. The standard $k - \epsilon$ model comprises of equation (3.15), (3.16) and (3.17). These equation along with equations (3.6) and (3.7) form a closed system for determining $\bar{u}_i$, $\bar{p}$, k, ϵ in an incompressible turbulent flow.

3.5   Non-Dimensionalisation of the Governing Equations

The variables are non-dimensionalised in the following manner

$$
\begin{aligned}
\bar{U} &= \frac{\bar{u}}{U_0},\ \bar{V} = \frac{\bar{v}}{U_0},\ \bar{W} = \frac{\bar{w}}{U_0},\ X = \frac{x}{H}\\
Y &= \frac{y}{H},\ Z = \frac{z}{H},\ \bar{P} = \frac{\bar{p} - p_0}{\rho U_0^2},\ t = \frac{t}{H/U_0}\\
k_n &= \frac{k}{U_0^2},\ \epsilon_n = \frac{\epsilon}{U_0^3/H},\ \nu_{t,n} = \frac{\nu_t}{\nu}
\end{aligned}
\tag{3.18}
$$

where U_0, H, p_0 are some charectristic scale of velocity, length, pressure, respectively and ν is the kinematic viscosity. The equations are then transformed to

- **Continuity equation**

$$
\frac{\partial \bar{U}}{\partial X} + \frac{\partial \bar{V}}{\partial Y} + \frac{\partial \bar{W}}{\partial Z} = 0
\tag{3.19}
$$

- **Momentum equations**

  The compact form of the moementum equation in non-dimensionalised manner is

$$
\begin{aligned}
\frac{\partial \bar{U}_i}{\partial t} + \bar{U}_j \frac{\partial \bar{U}_i}{\partial x X_j} = & -\frac{\partial}{\partial X_j}\left(\bar{P} + \frac{2}{3}k_n\right)\\
& + \frac{1}{Re} \cdot \frac{\partial}{\partial X_i}\left[(1 + \nu_{t,n})\left(\frac{\partial \bar{U}_i}{\partial X_j} + \frac{\partial \bar{U}_j}{\partial X_i}\right)\right]
\end{aligned}
\tag{3.20}
$$

  where Reynolds number $Re = U_0 H/\nu$

- **k equation**

$$
\begin{aligned}
\frac{Dk_n}{Dt} = & \frac{1}{Re}\frac{\partial}{\partial X}\left[\left(1 + \frac{\nu_{t,n}}{\sigma_k}\right)\frac{\partial k_n}{\partial X}\right] + \frac{1}{Re}\frac{\partial}{\partial Y}\left[\left(1 + \frac{\nu_{t,n}}{\sigma_k}\right)\frac{\partial k_n}{\partial Y}\right]\\
& + \frac{1}{Re}\frac{\partial}{\partial Z}\left[\left(1 + \frac{\nu_{t,n}}{\sigma_k}\right)\frac{\partial k_n}{\partial Z}\right] + G_n - \epsilon_n
\end{aligned}
\tag{3.21}
$$

where the nondimensional production term is

$$
\begin{aligned}
G_n = \frac{\nu_{t,n}}{Re} \Bigg[& 2\left(\frac{\partial \bar{U}}{\partial X}\right)^2 + 2\left(\frac{\partial \bar{V}}{\partial Y}\right)^2 + 2\left(\frac{\partial \bar{W}}{\partial Z}\right)^2 \\
& \left(\frac{\partial \bar{U}}{\partial Y} + \frac{\partial \bar{V}}{\partial X}\right)^2 + \left(\frac{\partial \bar{V}}{\partial Z} + \frac{\partial \bar{W}}{\partial Y}\right)^2 + \left(\frac{\partial \bar{W}}{\partial X} + \frac{\partial \bar{U}}{\partial Z}\right)^2 \Bigg]
\end{aligned} \quad (3.22)
$$

- ϵ equation

$$
\begin{aligned}
\frac{D\epsilon_n}{Dt} = & \frac{1}{Re}\frac{\partial}{\partial X}\left[\left(1+\frac{\nu_{t,n}}{\sigma_\epsilon}\right)\frac{\partial \epsilon_n}{\partial X}\right] + \frac{1}{Re}\frac{\partial}{\partial Y}\left[\left(1+\frac{\nu_{t,n}}{\sigma_\epsilon}\right)\frac{\partial \epsilon_n}{\partial Y}\right] \\
& + \frac{1}{Re}\frac{\partial}{\partial Z}\left[\left(1+\frac{\nu_{t,n}}{\sigma_\epsilon}\right)\frac{\partial \epsilon_n}{\partial Z}\right] + C_{\epsilon1}\frac{\epsilon_n}{k_n}G_n - C_{\epsilon2}\frac{\epsilon^2}{k_n} \quad (3.23)
\end{aligned}
$$

and the non-dimensionalised eddy viscosity $\nu_{t,n}$ is

$$
\nu_{t,n} = C_\mu Re\frac{k_n^2}{\epsilon_n} \quad (3.24)
$$

equation (3.19 - 3.23) constitue the full set of equations which need to be solved with the relation (3.24) to obtain the mean flow filed.

3.6 Boundary and Initial Condition for Turbulent Flows

The partial differential equation (3.19 - 3.23) need appropriate initial and boundary conditions to yield unique and physically meaningful solutions.

Boundary Condition

The inlet condition for the mean velocity can be specified using any physically reasonable profile. For velocity we can prescribe a uniform profile $\bar{U} = U_0$ ad the inlet value of the velocity, or a fully developed channel velocity profile can be specified. One may perhaps specify the 1/7 power law velocity profile at the inlet. The specified velocity profile at the inlet depends on the type of flow

beign simulated. Typically the transverse velocity components i.e., $\bar{V}$ and $\bar{W}$ are prescribed as zero at the inlet. As for pressure, the gradient of Presurre may be set to zero

$$\frac{\partial \bar{P}}{\partial X} = 0 \tag{3.25}$$

The turbulent kinetic energy k_n and its dissipation rate are calculated from the value of turbulent intensity specified at the inlet as follows:

$$k_{in} = 1 \cdot 5 \left(U_{in} I \right)^2, \tag{3.26}$$

where I is the turbulent intensity, and

$$\epsilon_{in}(Y) = \frac{k_n^{3/2} C_\mu^{3/4}}{\chi Y} \quad \text{for } Y < (\lambda/\chi) \tag{3.27}$$

$$= \frac{k_n^{3/2} C_\mu^{3/4}}{\lambda} \quad \text{for } Y > (\lambda/\chi) \tag{3.28}$$

where $\chi = 0.42$ which is known as von Karman constant, λ is a constant usually taken to be equal to 0.09. and Y is the normal distance from the wall.

Often the turbulence quantities of the domain are uncertain and one is forced to estimate these quantities as best as possible. In general the inlet turbulence intensity and characteristic length are a function of flow details upstream. A very quiescent flow upstream might yield an inlet turbulence intensity of $2-3\%$ (i.e. I=0.02-0.03). If the upstream flow involves flow over a rough edges or turning, the inlet value intensity may be as high as $10-14\%$. A range of k_{in} and ϵ_{in} are used in the literature but for most modelling applications the prediction are found to be insensitive to these values (Luo[26]) and this insensitivity was also observed in the channel flow simulations done in this study.

At the outlet boundary the gradients of the quantities along the direction of flow can be set to zero.

$$\frac{\partial \bar{U}}{\partial X} = \frac{\partial \bar{V}}{\partial X} = \frac{\partial \bar{W}}{\partial X} = \frac{\partial \bar{k}_n}{\partial X} = \frac{\partial \bar{\epsilon}_n}{\partial X} = 0 \tag{3.29}$$

The pressure at outlet boundary was set to zero. Details regarding the boundary condition at the wall for velocity, k and ϵ are discussed in the next section which describes the near walltreatment for these computations.

Initial Condition

In this sudy, we are interested in only the steady state solutions and times stepping is only the false transient means of obtaining the final state. Thus the initial conditions are prescribed quite arbitrarily as the steady solution doesn't depend upon them. The initial condition for velocities can be set to zero over the entire domain, pressure is also set to zero initialy. For the turbulent kinetic energy and dissipation rate, the inlet values were taken as initial condition.

3.7 Near Wall Treatment

The velocity variation near a wall in the a turbulent flow has typical features. The velocity distribution shows essential differences in the three different regions.

1. the viscous sublayer ($Y^+ < 11$)

2. the Log-law region ($11 < Y^+ < 70$)

3. the fully turbulent region ($Y^+ > 70$)

where Y^+ is the nondimensional distance to the wall and is expressed as $Y^+ = \frac{U_\tau Y}{\nu}$

In the viscous sublayer the flow is dominated by the viscous effects and the turbulent effects are negligible i.e. the contribution from the turbulent

friction can be completely neglected compared to laminar friction. In the Log-law region both contributions are comparable, whereas in fully turbulent region the laminar contribution is negligible compared with turbulent friction.

For high Reynolds number flows the value of Y^+ may range above 1000. The thickness of the viscous sublayer is very small compared to the width of the whole domain. However significant changes in velocity as well as temperature occur in the viscous sublayer it is very important that this region be taken into account while performing the computations. This would mean that we must take the computational grid small enough to represent the sublayer with accuracy but require much computer memory and time (as done in Low-Reynolds number $k - \epsilon$ model). Another alternative is to allow a coarser grid points in the sublayer, but to simulate the effects of the sublayer and the log-law region using the laws of the wall. This is the approach taken by he wall function treatment.

In the standard $k - \epsilon$ model the k and ϵ equation are applicable in the fully turbulent region ($Y^+ \geq 70$). So while using a $k - \epsilon$ model usual that the first grid point be placed at a distance $Y^+ > 30$, and the variables at the first grid point are specified by the wall function treatment discussed below.

(a) Momentum Equation
In the log-law region the universal velocity distribution may be written as

$$\frac{\bar{U}}{U_\tau} = \frac{1}{\chi} \ln Y^+ + 5.5 \tag{3.30}$$

or

$$\frac{\bar{U}}{U_\tau} = \frac{1}{\chi} \ln \left(E Y^+ \right) \tag{3.31}$$

where $U_\tau = \sqrt{\frac{\tau_w}{\rho}}$ is a friction velocity, χ the von Karman constant is 0.42 and $E = 9.0$ for smooth walls. Using this velocity profile we can compute the wall shear stress from the velocity y at first grid point outside the viscous sublayer.

This law is not valid in the region of stagnation and separation but then the wall stress has little influence on overall flow and thus the little effect on the prediction.

(b) Kinetic Energy

The Reynolds stresses in the region $30 < Y^+ < 100$ are nearly constant. In the region $30 < Y^+ < 100$, the convection and diffusion of $\overline{u_i' u_j'}$ are negligible so a local equilibrium prevails. This implies that the production and rate of dissipation of turbulent kinetic energy near the wall are equal i.e.

$$-\rho\overline{u'v'}\frac{\partial \bar{U}}{\partial Y} = \rho\epsilon \tag{3.32}$$

The Reynolds stresses in this region are nearly constant at the value τ_w.

$$\rho\overline{u'v'} = \tau_w \tag{3.33}$$

from this we can write

$$-\overline{u'v'} = \frac{\tau_w}{\rho} = \nu_t\frac{\partial \bar{U}}{\partial Y} \tag{3.34}$$

Inserting $\nu_t = C_\mu\frac{k^2}{\epsilon}$ in the above expression we get

$$-\overline{u'v'} = C_\mu\frac{k^2}{\epsilon}\frac{\partial \bar{U}}{\partial Y} \tag{3.35}$$

Substituing the value of $\frac{\partial \bar{U}}{\partial Y}$ obtained from (3.32) we get

$$\left(-\overline{u'v'}\right) = C_\mu\frac{k^2}{\epsilon}\frac{1}{\left(-\overline{u'v'}\right)} \tag{3.36}$$

or

$$k = \frac{U_\tau^2}{C_\mu^{1/2}} \tag{3.37}$$

in the nondimensional form equation (3.37) is

$$k_n = \frac{U_{\tau,n}}{C_\mu^{1/2}} \tag{3.38}$$

Equation (3.38) is used for calculating the kinetic energy at the near wall point.

(c) Dissipation Rate

In the log-law region, the local equilibrium of production and dissipation of turbulent kinetic (3.32) and the constancy of Reynolds stresses yield

$$\epsilon = \frac{\tau_w}{\rho}\frac{\partial \bar{U}}{\partial Y}$$
$$= U_\tau^2 \frac{\partial \bar{U}}{\partial Y} \tag{3.39}$$

From log-law (3.31) we obtain

$$\frac{\partial \bar{U}}{\partial Y} = \frac{U_\tau}{\chi Y} \tag{3.40}$$

Finally ϵ becomes

$$\epsilon_p = \frac{U_\tau^3}{\chi Y_p} = \frac{C_\mu^{3/4} k^{3/2}}{\chi Y_p} \tag{3.41}$$

in the nondimensional form equation (3.41) is written as

$$\epsilon_{p,n} = \frac{U_{\tau,n}^3}{\chi Y_p} = \frac{C_\mu^{3/4} k_n^{3/2}}{\chi Y_p} \tag{3.42}$$

where Y_p refers to the normal distnace from the wall . The equation (3.42) represents the value of the ϵ at the near wall point.

3.8 Implementation of $k - \epsilon$ Model

In this section we discuss the way in which the $k - \epsilon$ model has been implemented, mainly dealing with the the wall-function treatment and the algorithm for obtaining eddy viscosity.

The Reynolds averaged equation is solved over the entire domain with a modification when applied to the near wall point. The no-slip condition is imposed on the wall and the velocity at near-wall point is obtained from the velocity gradient computed fromm the wall shear stress:

$$\tau_w = \mu \frac{\partial \bar{u}}{\partial y} = \frac{\bar{u}\chi C_\mu^{1/4} k^{1/2}}{\ln(E y_P^+)} \tag{3.43}$$

where p refers to the first grid point near the wall. For the application of equation (3.43) it is very important that point p be at a distance of $y^+ > 11.63$.

For turbulent kinetic energy and dissipation rate equation (3.16) and (3.17) are solved in a domain far from the viscous sublayer i.e. above $y^+ > 30$. For the near wall point the values of k and ϵ are obtained through the use of equation (3.38) and (3.42) respectively. For a three dimensional turbulent flow u_τ is expressed as

$$U_\tau = \frac{\chi \bar{U}}{\ln(E y_p^+)} \qquad (3.44)$$

where $\bar{U}$ is the resultant velocity parallel to the wall

Solution Algorithm

1. Guess the initial velocity, k, ϵ and p. Initial values of k and ϵ has to be taken as given in section (1.6). The initial turbulent viscosity has to be computed from the initial values of k and ϵ.

2. Solve the momentum equations for the velocity at $(n+1)$ time level using the value of ν_t at (n) time level.

3. calculate the convection and diffusion fluxes for k and ϵ as described in chapter (2).

4. Calculate the source terms for k and ϵ

5. Obtain the values of k and ϵ at $(n + 1)$ time level by solving equation (3.16) and (3.17) at the points excluding the near wall points. Where n' refers to the psuedo time stepepping for k and ϵ equtaion. For the near wall points apply wall-function treatment.

6. Calculate the turbulent viscosity .

7. update the boundary values of k and ϵ.

8. Check for steady state by computing $r.m.s$ value given by

$$\phi_{rms} = \sqrt{\frac{\sum(\phi^{n+1} - \phi^n)^2}{N_{total}}} \qquad (3.45)$$

if $max(\phi_{rms}) \leq 10^{-3}$ goto step (2) else goto step (3).

In step (5) its important that the time step value (Δt) for k and ϵ equation has to be smaller than that for the velocity so as to minimize the occurence of negative values of k and ϵ (if some negative values of k and ϵ very small in magnitude occurs then their absolute value is considered).

Chapter 4

Results and Discussion

The code is tested on two flow configurations, namely, two dimensional channel flow and the flow over a backward facing step. The results are compared with the published computational results.

1. Channel Flow

The flow in a channel has been simulated for two different Reynolds numbers. (*i*) Re=6600 and (*ii*) Re=24000. The results due to Re=6600 are compared with the DNS results of Kim *et al.*[27] and those of the other Low-Reynolds number models of Chien[28], Shih and Monsour[29] and Jones & Launder[30]. The results for Reynolds number of 24000 have been compared with the experimental data of Laufer[31] and the numerical results of Goldstein[33] and Lam & Bremhorst[32].

For both the cases the Reynolds number is based on channel width. The flow configuration is shown in Figure (4.1). The boundary conditions of interest are

at the inlet:

$$\bar{U}_{in} = 1, \quad \bar{V} = 0$$
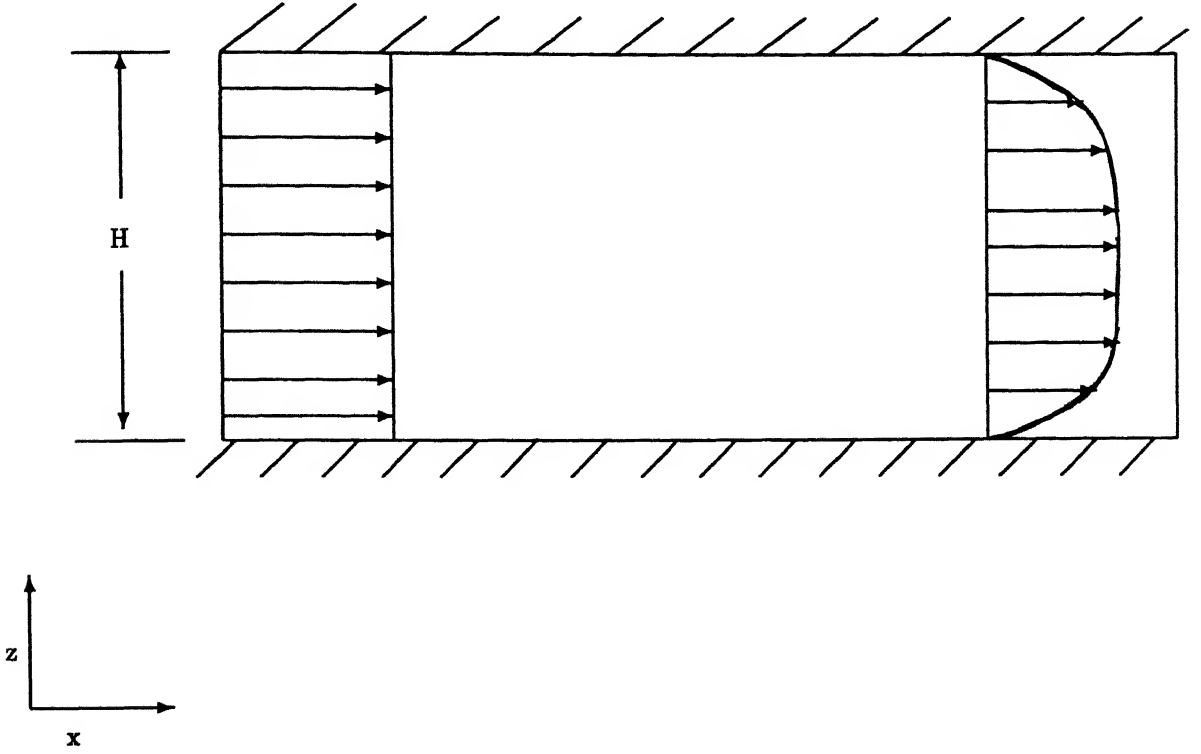
Figure 4.1: Turbulent flow through a channel

$$k_{in} = 1.5(U_{in}I)^2, \quad \text{where } I = 0.05$$

$$\epsilon_{in} = \frac{C_\mu^{3/4} k_n^{3/2}}{\lambda}, \quad \text{where } \lambda = 0.09$$

$$\frac{\partial \bar{P}}{\partial x} = 0$$

at the outlet the gradient of the dependent variables in the flow direction is set to zero except for pressure, which has the condition $P_{out} = 0$. At the top and the bottom boundaries $\bar{U} = \bar{V} = 0$, and k and ϵ the wall functions have been used

For the case of Reynolds number of 6600, the distribution of turbulent kinetic energy (Fig. 4.2) and the nondimensional turbulent viscosity (Fig. 4.3) is compared with the results of DNS[27] and the other two low Reynolds number models[32,33]. Figure 4.2 depicts that the near-wall variation of turbulent kinetic energy from present computation corroborates well with the DNS data. How-
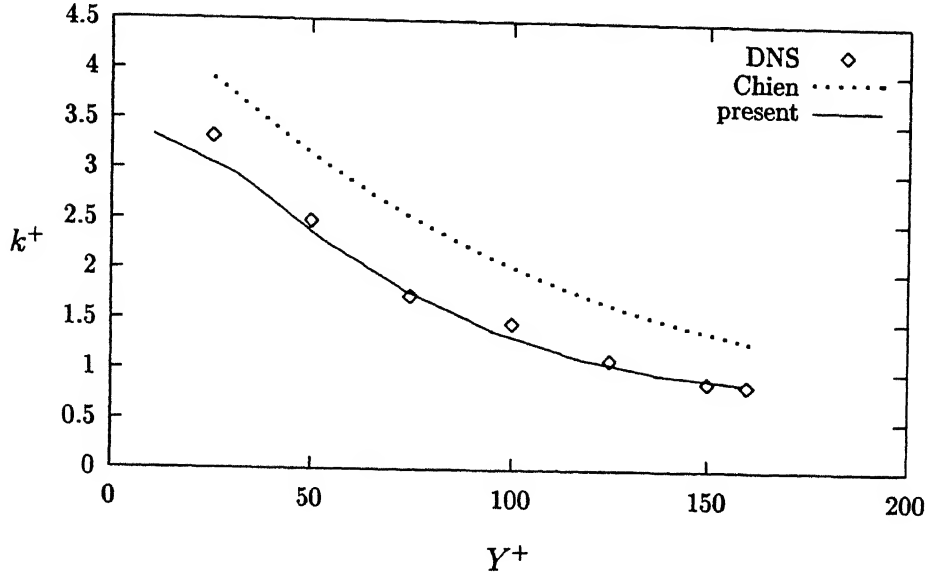
Figure 4.2: Near wall variation of turbulent kinetic energy for Re=6600
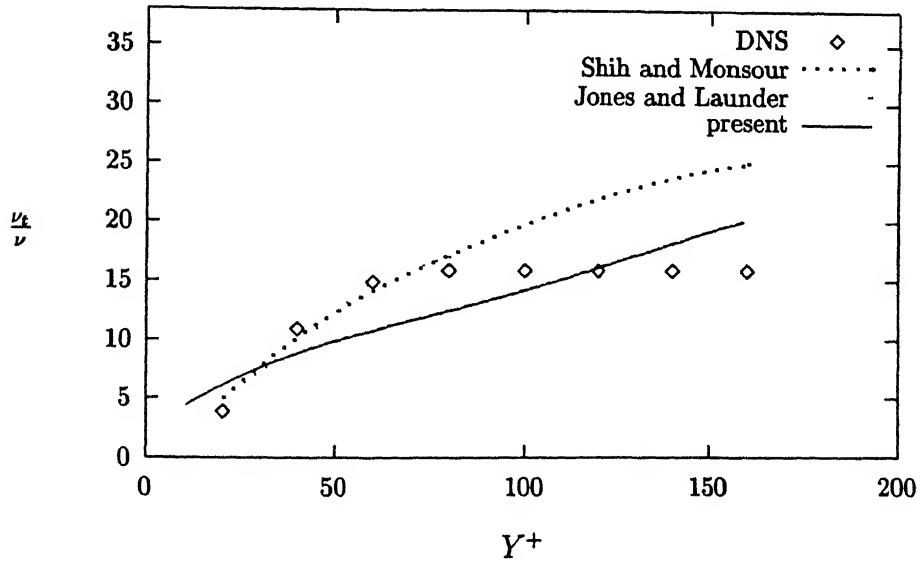
Figure 4.3: Near wall variation of eddy viscosity for Re=6600
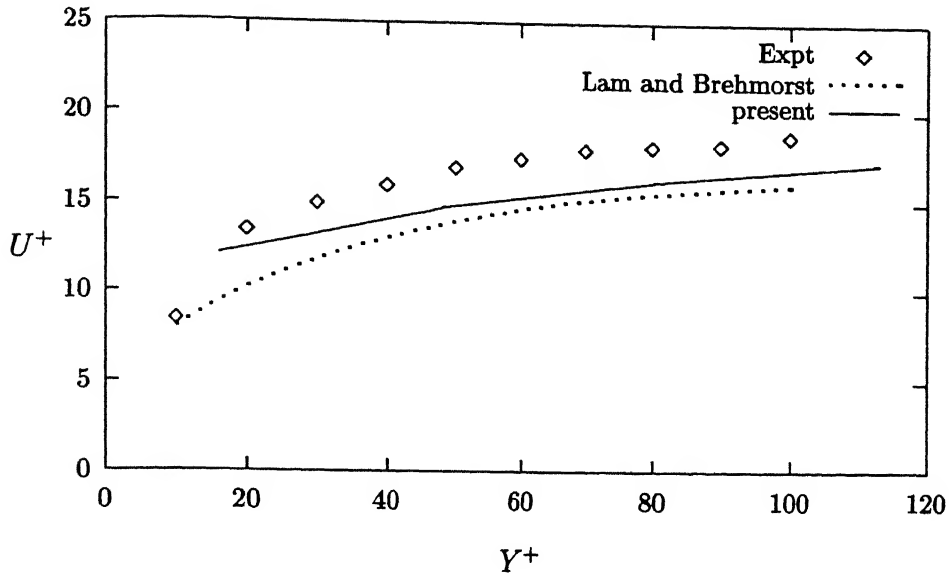
Figure 4.4: Near wall variation of velocity for Re=24000

ever, the variation of turbulent viscosity predicted by the present computation does not match the DNS data so well (Fig. 4.3). For the case of Reynolds number of 24000, the near wall distribution of tangential velocity (U^+) and kinetic energy k from the prsent computation is compared with the experimental results of Laufer[31] and the numerical results of Cho and Goldstein[33] and Lam & Bremhorst[32] in Figures 4.4 and 4.5. The predicted results agree well with the experimental results of Laufer[31] and the other numerical results of Goldstein[33].

2 Backward-Facing Step flow

Among the few selected flow situation that have been studied in detail is that of the flow over a backward facing step. It is often used as a test-case for flow solvers and turbulence models, since it embodies several difficult aspects of turbulent flows namely, flow seperation, reattachment, and the presence of the secondary recirculation regions.

A schematic of the basic flow field is shown in Figure (4.6). The flow seperates at the step corner and reattaches at a distance X_R from the step. This

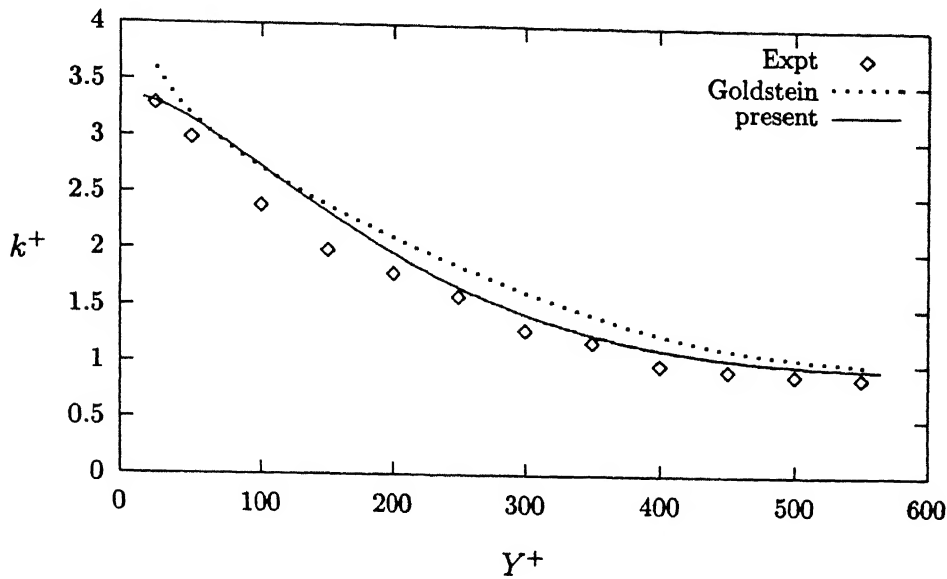Figure 4.5: Near wall variation of turbulent kinetic energy for Re=24000

distance is a function of the Reynolds number and the expansion ratio $\left(\frac{H_2}{H_1}\right)$. Several recent works (reference: 35-37) have studied the flow past a backward facing step and provide an excellent review of the current state of the art from both experimental and computational points of view. Among these, Speziale[34] have applied a non-linear model for predicting the fluid flow and has found that introducing of anisotropy in the model leads to reduction in the error of predicting the reattachment length. The work presented here shows some of the features of standard $k - \epsilon$ model as far the secondary recirculation zone is concerned.

The fully developed flow past a backward facing step with an expansion ratio of 3:2, at a Reynold number of 46000 based on step height is chosen as a the primary reference. The computation are performed with a 110×73 finite volumes. The domain here is resolved finely because many earlier computations had serious error of around 25-30% due to insufficient resolution (Thangam and Hur[38]). Regarding the boundary condition, a uniform velocity profile is prescribed at the inlet which is $11H$ length upstream of the step. The
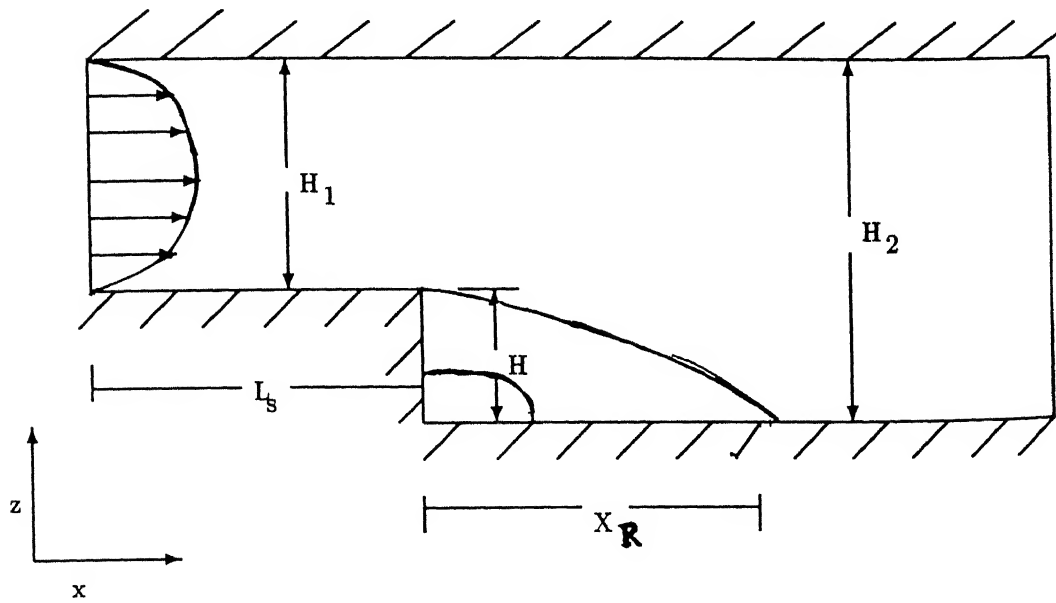
Figure 4.6: Flow past a backward facing step

turbulent intensity I is 0.1, for ϵ the inlet condition is specified as described in the channel flow problem. The downstream length is $24H$ so as to ensure fully developed condition. At the outlet boundary condition is as described in chapter3. No-slip boundary conditions for velocity and the wall function treatment for k and ϵ are used at the walls. The results obtained for the velocity are shown in Figure (4.7) with a comparison with the experimental results of Kim *et al.*[36], and the RNG results of Thangam and Speziale[37]. It was observed that a steady-state condition was not reached in the present computaions and that the flow remained guass-periodic as has been experimentally observed. Therefore the results shown in the figures are averages over a time cyle.

The comparison of Reynold stresses (τ_{xy}) is also made as shown in Figure (4.8) with the experimental results of Kim *et al.*[36], second-order closure model calculation of Cellinligil and Mellor[35], and the RNG calculation of Thangam and Speziale[38]. The Experimentas have not provided reliable data for Reynold stresses in the recirculation region and so a comparison in that region is not

$\bar{U}$

◇ Experimental (Kim *et al.*[36])
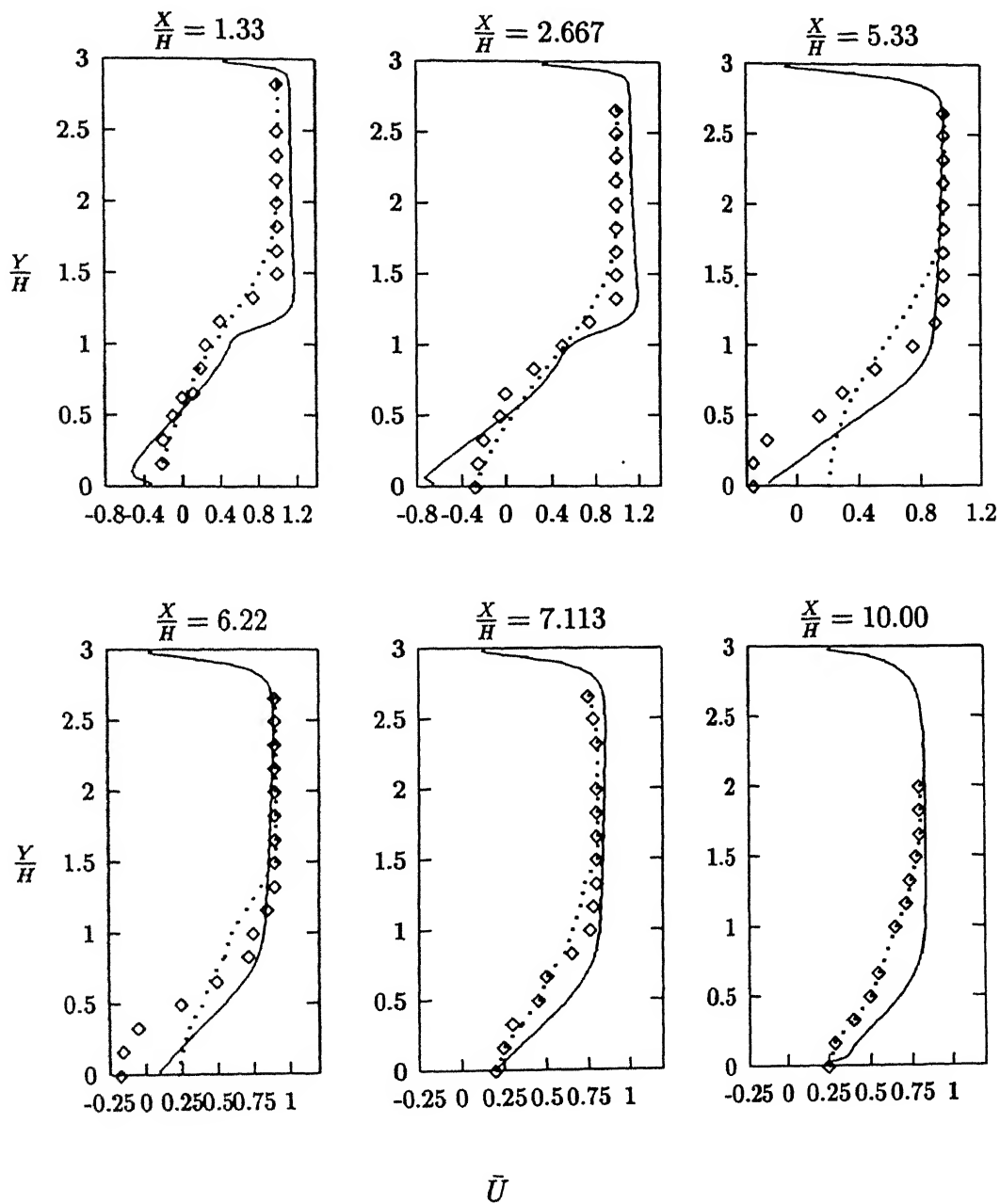... RNG (Speziale and Thangam[37])
— present

Figure 4.7: Comparison of flow field

made. The RNG model predicted a reattachment length of $6.0H$ while a second order model predicted a reattachment length of $7.7H$. and Thangam and Hur predicted the value of $5.58H$. The reattachment length found out by experiments is $7.0H$ and the reattachment length obtained by present computation is $6.0H$.

The present computation seems to have been able in capturing the secondary recirculation zone which other computations using the standard $k - \epsilon$ model failed(references:38,39). The length of secondary recirculation is also predicted well as $0.83H$, as compared to $1.0H$ obatined by Lien and Leschziner[39] with a Reynold stress transport model. The variation of velocity (Figure 4.9)near the bottom wall along the X direction shows the length of secondary and the primary recirculation zone.

Also a comparison of turbulent viscosity with the experimental data of Driver and Segmiller[40] and the computational results done by the same authors using a two equation model of Jones and Launder is shown in Figure (4.10). The vector plots are shown in Figure (4.11-4.12). Figure (4.12)shows the secondary recirculation region. Figure (4.13 and 4.14) shows the streamline plot for backwrad-facing step flow. Figure (4.14) also clearly shows the occurence of secondary recirculation. In fact a more fine grid may clearly show a tertiary eddy that seems to be nesting at the corner of the step. The computaional time taken by both the cases was 12.45 hours for channel flow and 67.20 hours for backward-facing step flow on a DEC Alpha-3000(version 2.2) dual processor machine.

Conclusion

A standard $k - \epsilon$ model is incorporated using a one layer near wall treatment in a Finite Volume code for flows in irregular geometries and is applied to two flow cases for validation with the following conclusions.

1) The code is been able to predict most of the quantities in a channel flow in

a good agreement with the experimental and DNS results.

2) The code is been able to solve the flow over a backward facing step in a good agreement with other published results.

3) The computations seem to capture secondary recirculation regions better than other attempts with the standard $k - \epsilon$ model.

4) More investigation has to be done to find out the appropriate reason for secondary recirculation near the step corner.
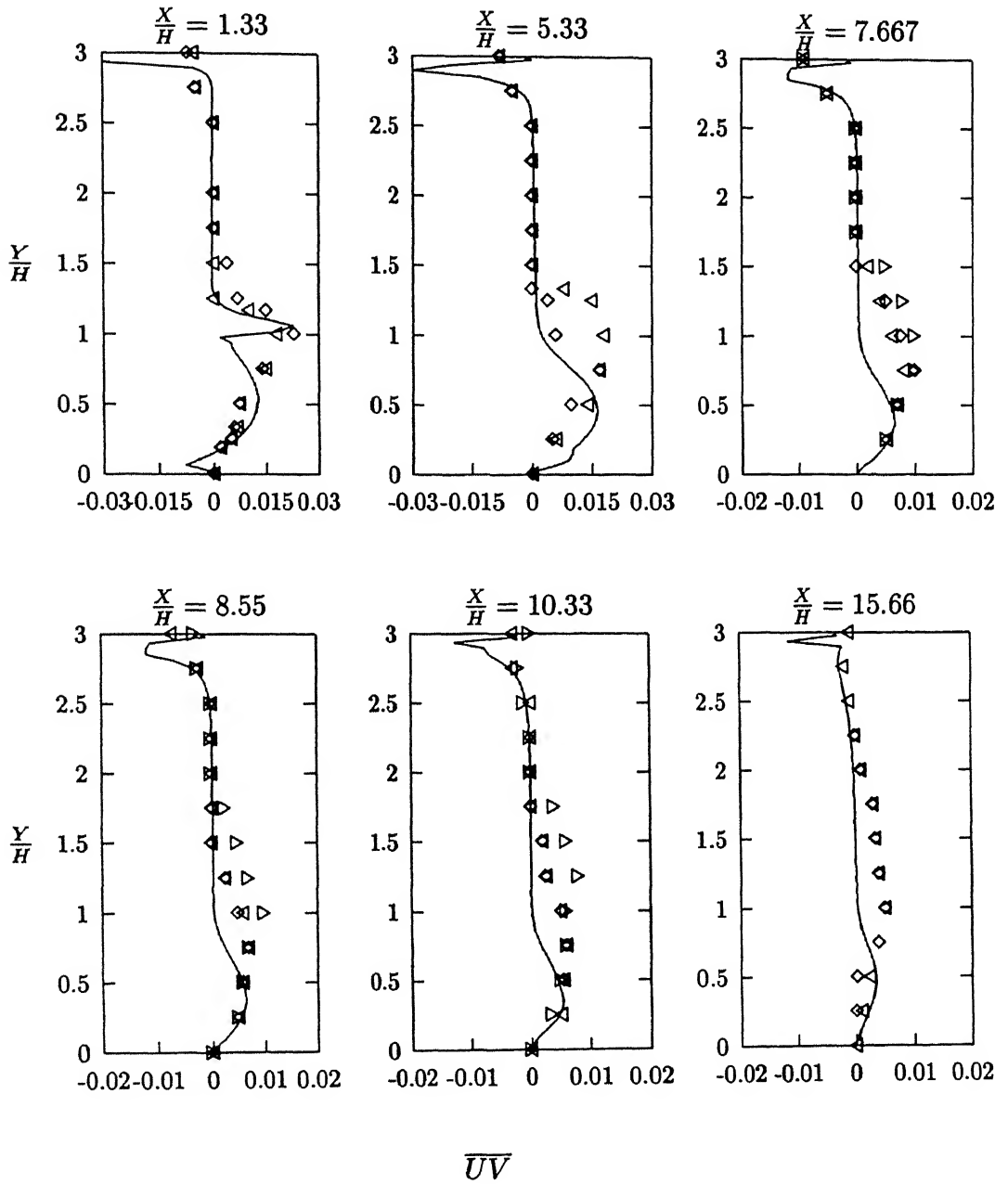
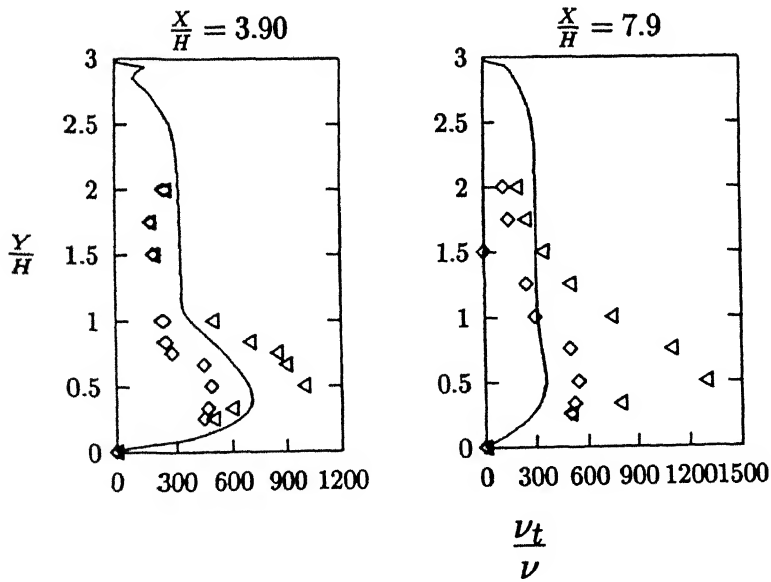Figure 4.8: Comparison of turbulent shear stresses
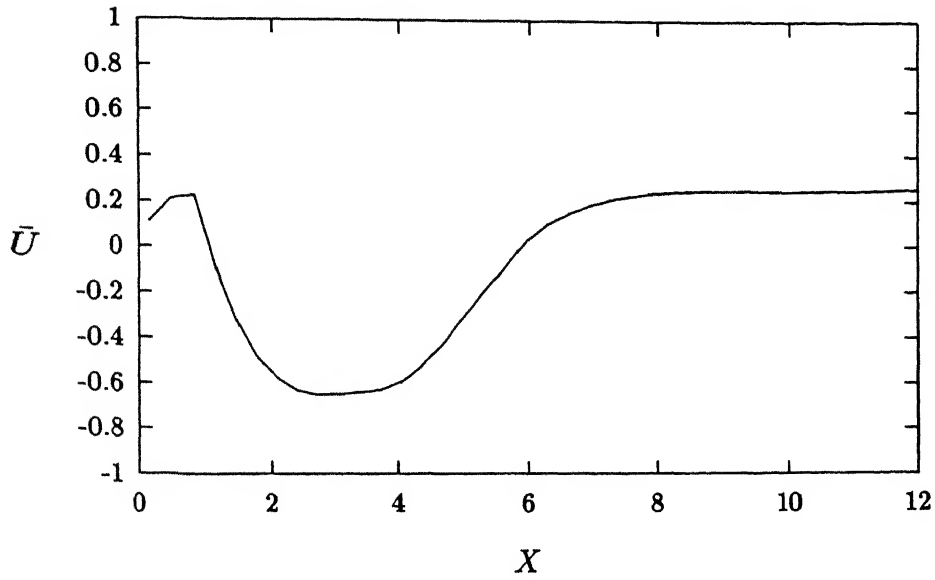
Figure 4.9: Variation of velocity near the bottom wall

◁   Low Reynolds number $k - \epsilon$ model (Jones and Launder[30])
◇   Experiment (Driver and Seegmiller[40])
___ present
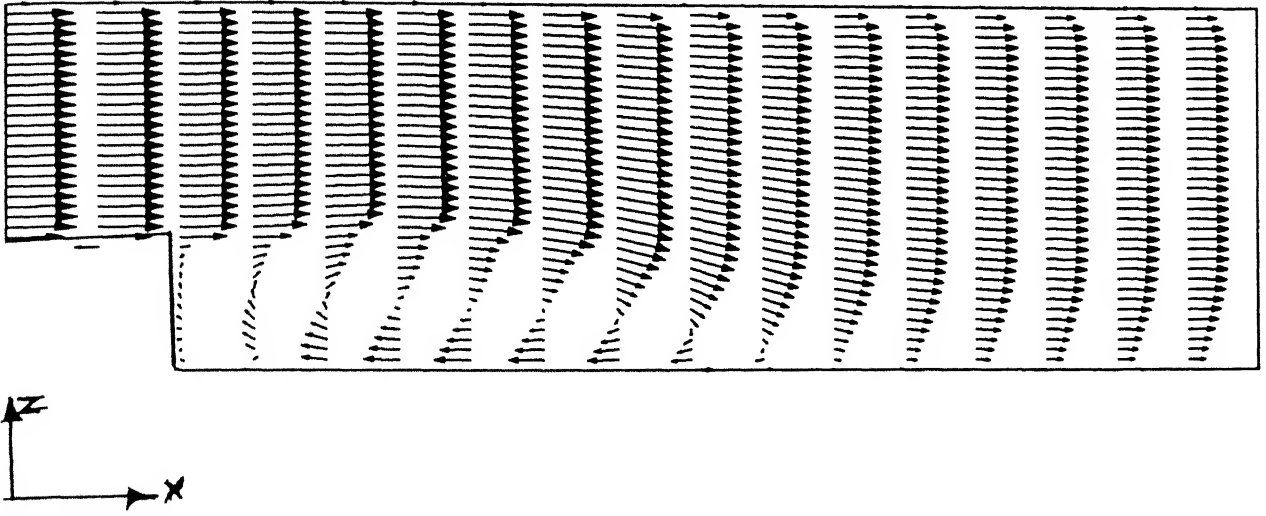
Figure 4.10: Distribution of eddy viscosity

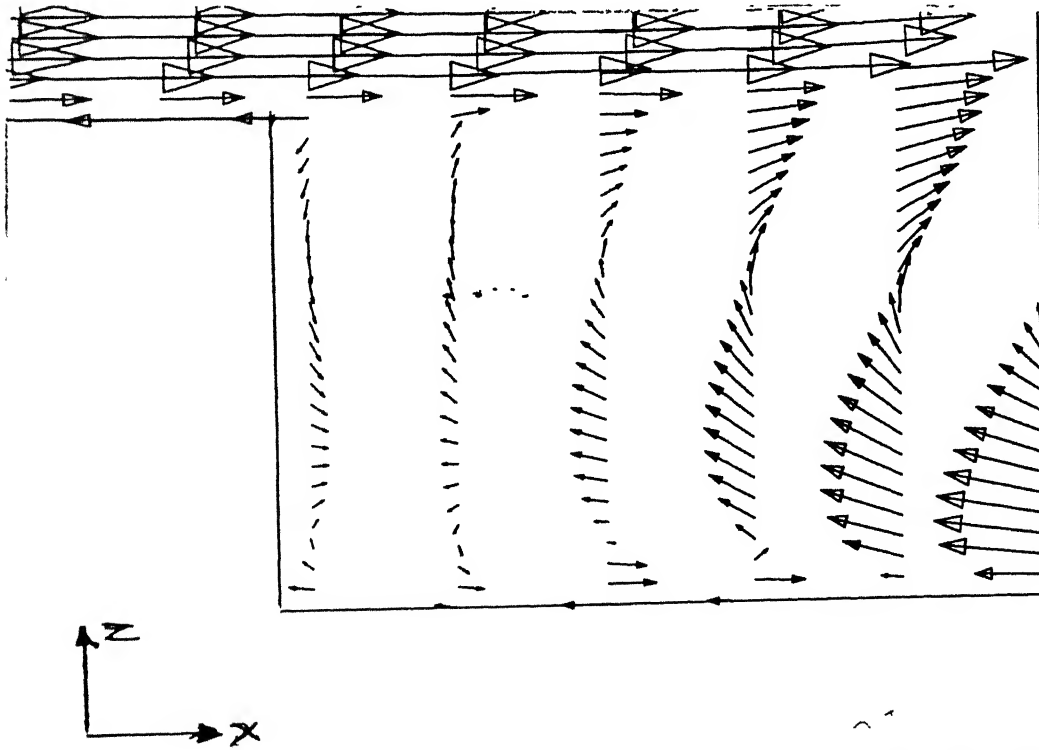Figure 4.11: Vector plot of flow past a backward facing step

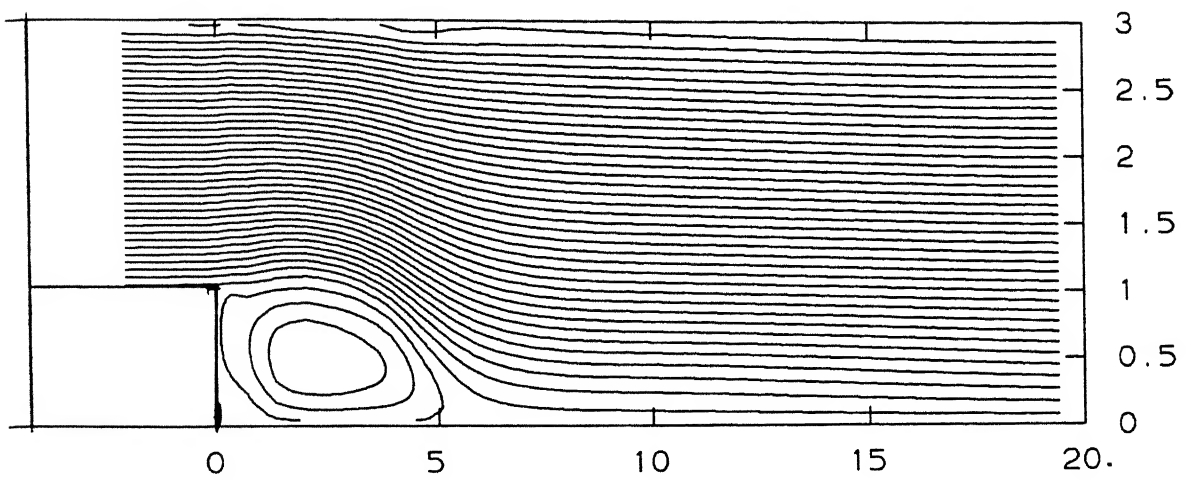Figure 4.12: Secondary recirculation near the step corener

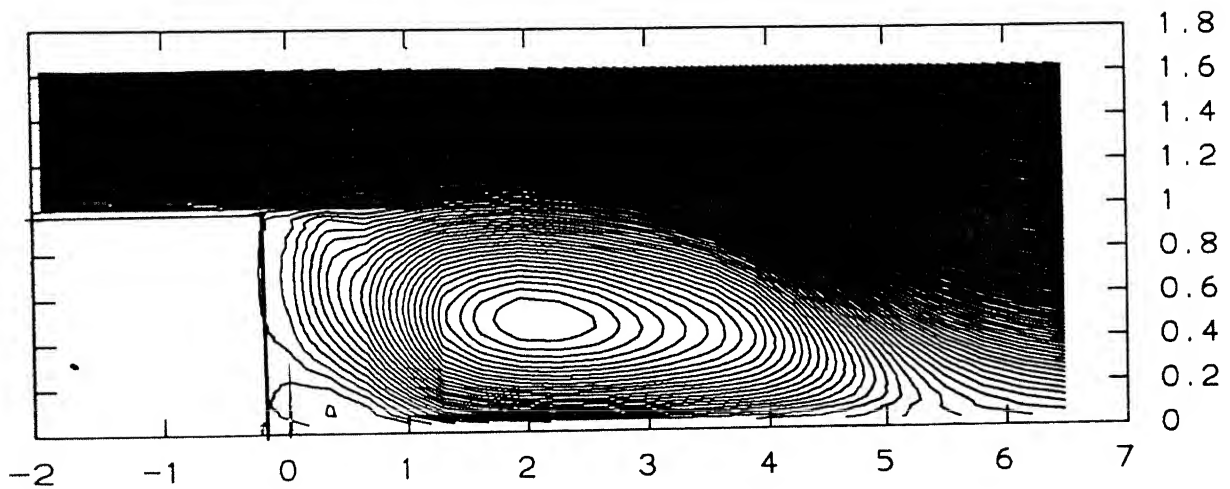Figure 4.13: Stream line plot for backward-facing step flow

Figure 4.14: Stream line plot showing the secondary recirculation region

Bibliography

[1] S. V. Patankar, *Numerical heat transfer and fluid flow*, Hemisphere, Washington, D. C., 1980.

[2] T. C. Huges and C. Taylor, *Finite Element Programming of the Navier Stokes Equation*, Pineridge Press, Swansea U. K., 1981.

[3] C. Hirsch, *Computation of Internal and External Flows*, John Wiley and Sons, 1987.

[4] S. B. Pope, "The Calculation of Turbulent Recirculating Flows in General Orthogonal Coordinates", *Journal of Computational Physics*, vol. 26, pp. 197 – 217, 1978.

[5] C. W. Rapley, "Turbulent Flow in a Duct With Cusped Corners", *International Journal of Numerical Methods in Fluids*, vol. 5, pp. 155 – 167, 1985.

[6] M. A. Habib and J. M. Whitelaw, "The Calculation of Turbulent Flows in Wide Angle Diffusers", *Numerical Heat Transfer*, vol. 5, pp. 145 – 164, 1982.

[7] T. Gal-chen and R. C. J. Somerville, "Numerical Solution of the Navier Stokes Equations with Topography", *Journal of Computational Physics*, vol. 17, 1975.

[8] M. Faghri, E. M. Sparrow, and A. T. Prata, "Finite Difference Solutions of Convection Diffusion Problems in irregular Domains using a Non-orthogonal Co-ordinates Transformation", *Numerical Heat Transfer*, vol. 7, pp. 183 – 209, 1984.

[9] S. Acharya and S. V. Patankar, "Use of an Adaptive Grid Procedure for Parabolic Flow Problems", *International Journal of Heat and Mass Transfer*, vol. 28, pp. 1057 – 1066, 1985.

[10] C. F. Hsu, *A Curvilinear Co-ordinate Method for Momentum Heat and Mass Transfer in Domains of Irregular Geometry*, Ph. D Thesis, University of Minnesota, 1981.

[11] C. M. Rhie, *A Numerical Study of Flow Past an Isolated Airfoil with Seperation*, Ph. D Thesis, University of illionis at Urbana - Champaign, 1981.

[12] M. Peric, *A Finite Volume Method for Prediction of Three Dimensional Fluid Flow in Complex Ducts*, Ph. D Thesis, Univ of London, 1985.

[13] A. Mukhopadhyay, T. Sundararajan, and G. Biswas, "An Explicit Transient Algorithm for Predicting Flows in Arbitary Geometry", *International Journal of Numerical Methods in Fluids*, vol. 17, pp. 975 – 993, 1993.

[14] A. K. Verma and V. Eswaran, "Overlapping Control Volume Approach for Convection Diffusion Problems", *International Journal of Numerical Methods in Fluids*, vol. 23, pp. 865 – 882, 1996.

[15] Satya Prakash, V. Eswaran, G. Biswas, and K. Muralidhar, *Numerical Simulation of Unsteady Three Dimensional Flow Around an Elongated Body Moving in an Incompressible Fluid Using a Parallel Computer*, DRDL Report No. 3, July 1996.

[16] W. Rodi, *Turbulence Models and their Application in Hydraulics - A State of Art Review*, IAHR, Delft, The Netherlands, 2nd Edition, 1988.

[17] V. Yakhot and S. A. Orszag, "Renormalization group Analysis of Turbulence, I. Basic Theory", *Journal of Scientific Computing*, vol. 178, pp. 3 – 51, 1986.

[18] C. G. Speziale, "On Nonlinear $k - l$ and $k - \epsilon$ Models of Turbulence", *Journal of Fluid Mechanics*, vol. 178, pp. 459 – 475, 1986.

[19] V. C. Patel W. Rodi and G. Scheuerer, "Turbulence Model for Near - Wall and Low Reynolds Number Flows: A Review", *AIAA Journal,*.vol. 23,No 9, pp. 1308 – 1318, 1985.

[20] K. Hanjalic and B. E. Launder, ", *Journal of Fluid Mechanics*, vol. 52, pp. 609, 1972.

[21] B. E. Launder and D. B. Splading, "The Numerical Computation of Turbulent Flows", *Computer Methods in Applied Mechanics and Engineering*, vol. 3, pp. 260–289, 1974.

[22] W. Kordulla and M. Vinokur, "Efficient Computation of Volume in Flow Predictions", *AIAA Journal*, vol. 21, pp. 917–918, 1983.

[23] P. K. Khosla and S. G. Rubin, "A Diagonally Dominant Second Order Accurate Implicit Scheme", *Computer and Fliuds*, vol. 2, pp. 207–209, 1974.

[24] R. S. Hirsh H. C. Ku and T. D. Taylor, "Pseudospectral Method for Solution of the Three Dimensional Incompressible Navier-Stokes Equation", *Journal of Computational Physics*, vol. 70, pp. 439–462, 1987.

[25] G. Biswas and V. Eswaran, *Short Term Course on Fundamentals and Modelling Aspects of Turbulent Flow*, Dept of Mechanical Engineering I.I.T Kanpur, 1995.

[26] X. L. Luo, "Operator Splitting Computation of Turbulent Flow in an Axisymmetric 180^0 Bend Using Several $k-\epsilon$ Models and Wall Functions", *International Journal of Numerical Methods in Fluids*, vol. 22, pp. 1189–1205, 1996.

[27] P. Moin J. Kim and R. Moser, "Turbulence Statistics in Fully Developed Turbulent Flow at Low Reynolds Number", *Journal of Fluid Mechanics*, vol. 117, pp. 123–166, 1984.

[28] K. Y. Chien, "Predictions of Channel and Boundary Layer Flows With a Low Reynolds Number Turbulence Model", *AIAA Journal*, vol. 20, pp. 33–38, 1982.

[29] T. H. Shih and H. N. Monsour, *Modelling of Near Wall Turbulence*, NASA TM 103222 ICOMP=90-17, 1990.

[30] W. P. Jones and B. E. Launder, "The Prediction of Laminarization with a Two Equation Model of Turbulence", *International Journal of Heat and Mass Transfer*, vol. 15, pp. 301–314, 1972.

[31] J. Laufer, *Investigation of Turbulent Flow in a Two Dimensional Channel*, NACA TM 1053, 1951.

[32] C. G. K. Lam and K. A. Bremhorst, "Modified Form of the $k-\epsilon$ Model for Predicting Near Wall Turbulence", *ASME Journal of Fluid Engineering*, vol. 103, pp. 456–460, 1981.

[33] H. H. Cho and R. J.Goldstein, "An Improved Low-Reynolds Number $k-\epsilon$ Model for Recirculating Flows", *International Journal of Heat and Mass Transfer*, vol. 37, pp. 1495–1508, 1993.

[34] C. G. Speziale and T. Ngo, "Numerical Solution of Turbulent Flow Past a Backward Facing Step Using a Non-Linear $k-\epsilon$ Model", *International Journal of Engineering Siences*, vol. 26, pp. 1099–1112, 1988.

[35] M. C. Cellenligil and G. L. Mellor, ", *ASME Journal of Fluid Engineering*, vol. 107, pp. 467, 1978.

[36] J. Kim, S. J. Kline, and J. P. Johnston, "Investigation of a Reattaching Turbulent Shear Layer: Flow Over a Backward-Facing Step", *ASME Journal of Fluid Engineering*, vol. 102, pp. 302–208, 1980.

[37] S. Thangam and C. G. Speziale, "Turbulent Seperated Flow Past a Backward-Facing Step: A Critical Evaluation of Two-Equation Model", *AIAA Journal*, vol. 29, pp. 1314–1320, 1992.

[38] S. Thangam and N. Hur, "A Higly Resolved Study of Turbulent Seperated Flow Past a Backward-Facing Step", *International Journal of Engineering Siences*, vol. 29, pp. 607–615, 1991.

[39] F. S. Lien and M. A. Leschziner, "Assessment of Turbulence Transport Models Including Non-Linear RNG Eddy-Viscosity Formulation and Second Moment Closure for Flow Over a Backward-Facing Step", *Computer and Fliuds*, vol. 23, pp. 983–1004, 1994.

[40] D. M. Driver and H. L. Seegmiller, "Features of Reattaching Turbulent Shear Layer", *AIAA Journal*, vol. 153, pp. 235–244, 1967.